RESEARCH FUNDED BY THE REGIONAL TRANSIT BOARD THROUGH THE CENTER FOR TRANSPORTATION STUDIES, UNIVERSITY OF MINNESOTA

REGIONAL TRANSIT BOARD

REMOTE SENSING OF PARTICULATE EMISSIONS FROM HEAVY-DUTY VEHICLES, PHASE 1

David Hofeldt,
Timothy Prochnau,
and Guoguang Chen,
Mechanical Engineering

CENTER FOR TRANSPORTATION STUDIES

UNIVERSITY OF MINNESOTA

REMOTE SENSING OF PARTICULATE EMISSIONS FROM HEAVY -DUTY VEHICLES

Final Report on Phase I

Submitted to

The Regional Transit Board

St. Paul, Minnesota

by

David L. Hofeldt, Timothy J. Prochnau, and Guoguang Chen

September 20, 1994

ACKNOWLEDGEMENTS

The work described herein was supported by the Regional Transit Board of St. Paul, Minnesota. The structure of this report follows that of Timothy J. Prochnau's master's thesis, "Development of a Remote Sensing System for Measuring Particulate Emissions from Heavy-Duty Vehicles," submitted to the Department of Mechanical Engineering, University of Minnesota, April, 1994. Several corrections and additions were made to the theoretical discussion. The engine measurements are completely new; the data was acquired by Guoguang Chen, with assistance from Imad Abdul-Khalek and Yong Chen.

TABLE OF CONTENTS

EXECUTIVE SUMMARY

This report summarizes the results of initial tests of a remote sensing system capable of real-time detection of particulate emissions from heavy-duty transit vehicles under actual on-road operating conditions. The technique employs optical extinction (sometimes called opacity) to measure concentrations of CO_2 and soot in the exhaust plumes from individual vehicles. Two wavelength regions (bands) are used, one of which is sensitive to soot and the other of which is used to monitor CO_2 levels. From these two measurements, an emissions index can be computed which normalizes the mass of soot emitted by the amount of fuel burned.

The primary goal of phase I was ascertain whether the new technique held promise of sufficient sensitivity and accuracy for on-road deployment. Thus, laboratory calibration experiments were carried out to evaluate the sensor response. An absorption cell was built to enable calibration of the instrument response in the CO_2 band. Subsequent experiments revealed that a single bandpass filter was not sufficient to limit sensor response to the CO_2 band alone. This is important, as water vapor and soot in actual vehicle exhaust plumes would interfere with the CO_2 measurement. A second overlapping bandpass filter has been ordered to correct this problem.

Measurements of CO_2 and soot concentrations were then made in a stationary exhaust plume taken directly from a laboratory engine. It is relatively easy to detect the presence of soot in engine exhaust, but it is relatively difficult to independently quantify the soot mass concentration. This is true even with multi-million-dollar dilution tunnel systems of the kind used for EPA certification by engine manufacturers. Since we did not have such a system at our disposal, a significant effort was expended to install a mini-dilution tunnel apparatus with the capability of measuring the soot mass concentrations. This system was capable of making both total particulate and nonvolatile particulate mass concentration measurements, and hence was used to calibrate the instrument response to soot. Although the values obtained may differ slightly from those

that would be obtained with a full-scale dilution tunnel, the results obtained here should be sufficient to understand the basic instrument performance.

Qualitative agreement was obtained between the soot and CO_2 concentrations measured with the remote sensing extinction technique and those measured with laboratory sampling instruments. Absolute concentrations were difficult to obtain due to variations in the turbulent mixing of the exhaust plume, but ratios between the soot mass concentration and the CO_2 mass concentration show the expected behavior. The ratios are the quantities which are needed to calculate a particulate emissions index for the engine in units of mass of particulate emitted per unit mass of fuel burned. High polluting vehicles can then be identified in comparison to other similar vehicles operating under similar conditions.

Several sources of uncertainty were identified in the initial tests, and modifications are being made for phase II. These are discussed in more detail in the text, but can be summarized as follows: 1) a second filter is required to increase sensitivity to CO_2 and reduce interference from soot; 2) better regulation of the 12 volt lamp power supply is needed; and 3) a corner cube retro-reflector should be used to facilitate alignment.

1.0 INTRODUCTION

1.1 REMOTE SENSING OF VEHICLE EMISSIONS

The last few decades have seen a dramatic shift in emphasis concerning vehicle emissions. Since the creation of the EPA in 1970, air pollution legislation has become increasingly stringent: engine manufacturers have had to drastically reduce vehicle emissions, and certain urban regions have been required to implement oxygenated fuels and inspection/maintenance programs in an effort to improve ambient air quality.

Current vehicle emissions regulations fall under two categories: light-duty vehicles (passenger cars and light trucks) and heavy-duty vehicles (trucks and buses). Restrictions for other engine categories are soon to be added. Light-duty vehicle emissions are specified in grams per mile (g/mi), whereas heavy-duty vehicle emissions are specified in grams per brake horsepower-hour (g/bhph) to account for the wide range in heavy-duty engine power outputs. Gas phase emissions were the focus of initial regulations and continue to be lowered, while particulate emissions from heavy-duty vehicles came under regulation in 1988 and have already been reduced sixfold.

Historically, the most common methods of determining vehicle emission contributions to ambient air quality have been modeling. and roadside measurements. The current EPA computer model, MOBILE5, assumes that the actual vehicle emissions are well-correlated with those from the Federal Test Procedure (FTP), a detailed transient chassis dynamometer test designed to simulate a typical summertime commute in Los Angeles [U.S. EPA 1993]. The accuracy of this assumption is suspect under driving conditions which vary from those encountered in the FTP test--for example, operation in cold climates, or hard accelerations employed for merging into or maneuvering within freeway traffic. Moreover, emissions from alternative-fueled vehicles can be substantially different from those of conventional gasoline- or diesel-powered vehicles.

The advantage of roadside measurements is that they measure the impact on air quality associated with local conditions, be they related to meteorological effects, vehicle age, traffic control, road conditions, operator personality or mood, or any of a number of

other effects. Such information can serve to locate problem areas or conditions as well as particular high polluting vehicles which can cause significant degradation in ambient air quality. This information is necessary if one is to develop and implement effective public policies which provide significant improvement in ambient air quality. Moreover, the data can be used to analyze the validity of model assumptions; this is necessary because modeling the dilution of the exhaust plumes in the atmosphere is a very difficult problem, and estimates often do not agree very well with roadside data.

Typical roadside measurements are conducted with point sensors which take air samples near a roadside at a given location and analyze them to determine pollutant concentrations, similar to the EPA carbon monoxide, ozone, and particulate sensors used to monitor compliance with ambient air quality standards. These give an indication of vehicle emissions averaged over a certain time or space interval at a given area, but they are influenced by local dispersion and mixing rates which exist at the time of the measurement. In general, such measurements cannot distinguish emissions from individual vehicles; thus, they are capable of monitoring the effects and possibly some of the causes of pollution levels, but they cannot be used to monitor how individual vehicles comply with emission standards.

Monitoring and enforcing of individual light-duty vehicle emissions are typically performed with idle emissions tests conducted in conjunction with vehicle inspection/maintenance (IM) programs. Unfortunately, the correlation between the current idle test measurements and actual vehicle emissions under load is not very good, as can be seen in the figure below (Haskew *et al.*, 1994). Note particularly that many vehicles register zero CO emissions during the idle test, but that emissions measured from the same vehicles undergoing FTP tests took on a wide range of values. It is also interesting to note that only 13 of 328 vehicles tested (4%) failed the idle test, and that those that did fail were just as likely to have met the FTP regulations as they were to have exceeded them. On the other hand, almost half the vehicles exceeded the emission standards for the loaded FTP test. Thus, a large amount of time, effort, and money is being spent to conduct inspection and maintenance programs which would seem to do

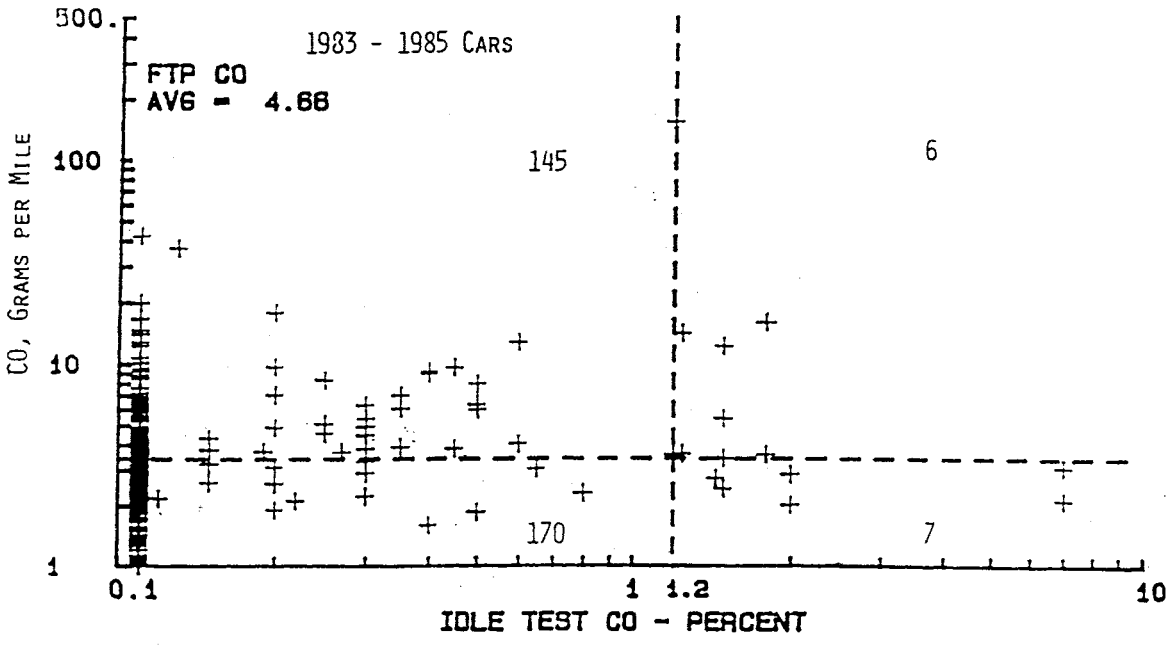

Fig. 1.1: Comparison of volume concentrations measured under idle test conditions in a typical inpection and maintenance program to results from loaded tests of the same vehicles conducted in accordance with the Federal Test Procedure. The dashed lines represent the current regulatory limits established for each test, and the numbers in each quadrant established by the regulations represent the number of vehicles tested which fell within the regions established by both regulations. [Haskew *et al.*, 1987].

little to guarantee improvements in ambient air quality (see also Scherrer and Kittelson, 1994).

Real-time pollution measurements of moving vehicles can only be obtained from specially-instrumented vehicles which can monitor their own emissions (a controlled fleet), or from remote sensing of vehicles (ideally a random fleet). The former are very costly, and there is no hope of obtaining measurements across a statistically significant fraction of the vehicle fleet. Remote sensing offers the possibility of measuring pollution from thousands of vehicles per day, enabling a statistically significant sample to be taken.

Several studies using remote sensing have been performed on light-duty vehicles since the first published data were taken in 1987 [Bishop et al. 1989]. First it is important to verify that the method works. A pilot study performed by the California Air Resources

Board (CARB), General Motors Research Laboratories, and the University of Denver (DU) equipped a 1989 Pontiac Bonneville SSE with a CO exhaust analyzer at the tailpipe. In addition, a computer interface with the engine computer allowed direct reading of vehicle speed and engine RPM, as well as direct control of the air/fuel ratio and subsequently CO output. This car was then driven past the CO remote sensing unit (called FEAT--Fuel Efficiency Automobile Test) at different air/fuel ratios and thus different CO emissions. An independent CARB observer on board directly controlled the air/fuel ratio and measured CO emissions without the driver's or the FEAT operator's knowledge of the tailpipe emissions--a "double-blind" experiment. The correlation coefficient between tailpipe and FEAT measurements was 0.97 for 34 data points, with an average tailpipe to FEAT ratio of 1.05 [Lawson et al. 1990]. Ambient temperature did not appear to limit the technique, for although the ambient temperatures were not published, measurements were taken both in Denver in January [Stephens et al. 1990, 1991] and in Mexico City in February [Beaton et al. 1992].

Additional studies performed with this type of system have yielded some revealing findings (see Table 1.1). The study by Lawson et al. took FEAT measurements on 2771 vehicles over two days. Of these, roughly 80% passed internal data reliability checks and were considered valid measurements, with a reported measurement accuracy of 10%. These measurements indicated that 10% of the vehicles produced about 55% of the CO emitted per gallon of fuel burned. To see if the FEAT instrument was predicting false high or low values, ten vehicles with less than two percent measured CO and 50 vehicles with over two percent measured CO were pulled over for a roadside inspection and tailpipe measurements of CO and HC emissions. Because vehicles in cold start mode can emit high CO, each driver was asked how long and how far the vehicle had been driven prior to testing. FEAT had an 80% success rate predicting that the vehicle would fail both CO and HC for the California Smog Check, and a 100% success rate in predicting that it would fail the CO portion of the test [Lawson et al. 1990].

A similar study by the EPA used remote sensing to measure both CO and HC emissions from thousands of in-use vehicles. Selected vehicles identified as high emitters

Table 1.1: Previous Remote Sensing Measurements		
PUBLICATION	LOCATION	FINDINGS
Ingalls 1989	Van Nuys, CA	Models underpredicted CO, HC, and PM2.5 emissions in tunnel by factors of about 3, 4, and 5, respectively
Bishop et al. 1990	Denver	7-10% of vehicles emitted 50% of CO 20% of vehicles emitted 80% of CO
Stephens et al. 1990, 1991	Denver	8.9% of vehicles emitted 50% of CO vehicles older than 1980 emitted 57% of CO
Lawson et al. 1990	Los Angeles	10% of vehicles emitted 55% of CO
Knapp 1991	Los Angeles	10 highest CO emitters over 20 times standard 10 highest HC emitters over 24 times standard 10 highest NOx emitters over 12 times standard
Hansen et al. 1990	Berkeley	20% of vehicles emitted 65% of BC

were pulled over and given an on-road inspection/maintenance test. A further subset of 76 vehicles were tested on a nearby portable dynamometer using the IM 240 driving cycle (a modified version of the Urban Dynamometer Driving Schedule of the Federal Test Procedure (FTP) lasting 240 seconds). Of these 76 vehicles, the study found that the 10 highest CO emitters were over 30 times the allowed standard of 7.0 g/mile and the 10 highest HC emitters were over 24 times the permitted standard of 0.41 g/mile. The dynamometer also showed that the 10 highest emitters of nitrogen oxides (NOx) were all more than 12 times the California certification standard of 0.4 g/mile. All of the top 10 CO emitters also failed the HC standard, and all but one (the worst) of the top 10 HC emitters failed the CO standard; in addition, eight of the top 10 CO emitters and eight of the top 10 HC emitters failed the NOx standard. Little or no correlation existed between any of the three pollutants and the vehicle model year in this relatively small fleet sample, although slight correlations existed between emitted pollutants and the measured fuel economy in miles per gallon [Knapp 1991].

The above tests give indications of the accuracy and reliability of monitoring emissions from individual vehicles via remote sensing, but this does not imply that remote sensing techniques can be performed without limitation. For example, several effects are

full load operating conditions can be on the order of 100 mg/m^3, whereas state-of-the-art engines are more like 30 mg/m^3. Concentrations of dry soot particles (the insoluble fraction) at idle are generally on the order of 1/10 of these, while concentrations during some acceleration transients may be 10 times higher or more. For a double pass through the center of a 4 inch diameter exhaust plume (L = 0.2 m) with M = 5 mg/m^3, the total extinction would be only about $e^{-0.011} = 1.1\%$. In typical absorption experiments in a laboratory, such small absorptions are relatively easy to measure using lock-in amplifiers or signal averaging techniques. However, the laboratory concentrations are generally steady, and long time constants can be employed to process the signals with high accuracy. In a remote sensing measurement, such long time constants are not possible because the plume passes by rapidly and is constantly diluting. Hence, 1% extinction might be about the best one could hope to accurately measure.

For the same configuration but with M = 500 mg/m^3, the transmitted energy would be only $e^{-1.1} = 33\%$, *i.e.* the extinction is 67%. The difference between the absolute and relative accuracies at these extremes can be illustrated by noting that a mass concentration of 10 mg/m^3 results in 2% extinction, whereas a mass concentration of 518 mg/m^3 results in a 68% extinction. At such high values of extinction, one must check that multiple scattering is not important. Multiple scattering occurs when light which is initially scattered out of the beam is scattered back toward the detector by a subsequent scattering event. This would effectively increase the measured transmission, and hence the mass concentrations would be underpredicted. Multiple scattering is somewhat less of a problem in strongly absorbing particulate fields because both the initial and secondary scattered light rays are strongly attenuated by absorption; a reasonable rule of thumb to use is that multiple scattering may be important when the scattering depth, $\overline{A}_{sca} ML \geq 0.3$. Since mass-specific scattering cross sections are on the order of 1/3 of mass-specific extinction cross sections in the visible part of the spectrum, the 500 mg/m^3 case is on the verge of multiple scattering difficulties. Hence, one would prefer to operate in a regime where extinction never exceeded 60%, which again requires some dilution during peak transients.

2.3 ABSORPTION BY CO_2

Extinction measurements are also employed to measure CO_2 concentrations in the exhaust plume. Mass concentrations of CO_2 vary directly with the amount of fuel burned, since almost all of the carbon in the fuel ends up as CO_2. Soot emissions are small by comparison, as are emissions of hydrocarbons and CO. Hence, measuring CO_2 concentrations gives an indication of the amount of fuel burned, assuming the chemical composition of the fuel is known. The primary difference between molecular extinction and particulate extinction is that molecules exhibit characteristic absorption bands, which are themselves composed of many individual absorbing lines. Absorption within these bands is orders of magnitude higher than molecular scattering, and hence scattering can be neglected (extinction = absorption). One of the characteristic absorption bands for CO_2 is centered in the mid-infrared at 4.2 μm. Although the absorption integrated across the entire band may not appear optically thick, the absorption at the centers of many of the individual lines may be. This means that the extinction will not be strictly exponential with increasing concentration-pathlength product (sometimes called the absorber thickness). Hence, calibration experiments are required to determine the system response.

An additional difficulty arises because soot particles also absorb at 4.2 μm, although not nearly as strongly as in the visible region. The average mass-specific extinction cross section integrated across a typical soot distribution at 4.2 μm is 1.3 m^2/g. Thus, the extinction due to soot particles will not be negligible, and the ability to measure CO_2 concentrations accurately will depend on the accuracy of the soot concentration measurements at the visible wavelength.

As with the soot measurement, it is important to ensure that the extinction produced by CO_2 in the plume lies within a reasonable range. Background concentrations of CO_2 in the ambient air may be important, and will be discussed in the next section. CO_2 comprises roughly 10% by volume of the exhaust gas at full load, which corresponds to about 14% by mass. If we assume the exhaust gas exits the stack at 500 °F (533 K), then the mass concentration (*i.e.* density) of CO_2 at the exhaust exit is about 100 g/m^3. The

mass specific absorption coefficient of CO_2 over a relatively small spectral region surrounding 4.2 μm is about 9.6×10^{-3} m^2/g. (The spectral region is selected by a bandpass filter with a full-width at half-maximum (FWHM) passband of about 50 nm.) Thus, at full load with a double pass across a 4 inch exhaust pipe, we would measure about a 20% drop in signal. Based on the discussion in the previous section, one might at first think this is too small for the full load case; however, one must recall that the CO_2 concentration is linear with fuel consumption, whereas soot concentration is not. Moreover, the range of CO_2 exhaust mass concentrations does not vary much from engine to engine. Hence, we only need to be able to measure CO_2 mass concentrations over a range of mass fractions of about 2 - 14% to be able to cover all operating conditions. Since the exhaust temperatures are cooler at light loads (approximately 400 °F = 478 K), the actual range of CO_2 mass concentrations in undiluted exhaust plumes is about 10 g/m^3 - 100 g/m^3. Hence, the extinction caused by the lowest CO_2 concentrations still lies above the 1% level used above.

2.4 EFFECT OF BACKGROUND CONCENTRATIONS

Thus far, assuming the 1% extinction sensitivity applies, we have been very fortunate that the range of extinctions caused by soot at 630 nm and by CO_2 at 4.2 μm both fall within acceptable ranges for a double pass through the center of an undiluted exhaust plume. However, the preceding discussion neglected the presence of particles and CO_2 in the ambient air. Such background concentrations will cause a background extinction level to exist on the signal. This has two effects: 1) the ability to measure small extinctions from the plume will now depend on the level to which the extinction in the ambient air remains constant over the time it takes us to take the measurement in the plume, and 2) the transmitted intensity will be lower, such that a more powerful illumination source may be needed to ensure that the signals reaching the detectors are adequate.

The combined extinction due to plume and ambient extinctions depends on how the plume mixes with the surrounding air after it exits the exhaust pipe. The situation is

equivalent to that of a pulsating jet exhausting into a cross flow, where the relative velocities between the jet and the cross flow depend on the exhaust flow rate and the vehicle velocity. Obviously, at some time after the vehicle passes, the plume will have undergone enough mixing with the surrounding air that it becomes essentially indistinguishable from the ambient air. In order to have the best sensitivity to the exhaust concentrations and minimize the effect of small fluctuations in the ambient extinction, measurements should be made as close as possible to the exhaust plume to maximize its effect relative to the ambient extinction.

The effective absorption thickness through the plume depends on dilution (you can't see a highly diluted plume against the background of the sky, but you can see it when it exits the exhaust pipe). In general, measurements will be made after some dilution has occurred because the beam must be positioned above the longest expected exhaust pipe length. The plume spreads due to mixing with the ambient air, which causes both an increase in the interaction length and a decrease in the plume concentration. As we noted earlier, the unknown dilution forces us to make a relative measurement, and fortunately the soot particles and CO_2 molecules behave similarly with regard to turbulent mixing. The integrated optical depth is an effective number which takes into account the increasing characteristic size of the plume and its concentration profile. Since the plume spreads out in two dimensions but the path length only increases along one, the integrated optical depth decreases with plume dispersion. At low vehicle velocities and high engine rpms typical of accelerations from a stop, the situation will be similar to that of a turbulent jet exhausting into a quiescent atmosphere. In this case, the integrated optical depth decreases roughly as the inverse of the distance from the jet exit, as long as the distance from the jet exit is greater than about 5 jet diameters. At higher vehicle velocities, the spread rate (*i.e.* rate of dilution) is difficult to predict in advance, although one might expect both high spreading rates as well as a few local chunks of fluid which have not undergone much dilution at all.

Estimating the combined extinction from ambient and exhaust plume aerosols requires some care. Before the exhaust plume, the ambient path length for a single pass is

just $L_a = L_{tot}$. Right at the exhaust port exit, the plume path length for a single pass would equal the exhaust pipe diameter, $L_p = D_{exh}$, assuming the beam cut through the center of the plume. The effective path length through the plume, L_p, could be less than this if either the beam diameter were of the same order as the plume diameter or if the beam did not cut across the plume on a diametral line. Similarly, right at the exit, the ambient air path length must be $L_a = L_{tot} - L_p$. Mixing between the air and the plume is what causes the plume to spread, such that the air concentration within the plume downstream of the exit is not zero. The concentration deficit decreases as the plume dilutes, such that the effective single pass path length through the ambient air tends back to $L_a = L_{tot}$. Thus, although the background extinction before and within the plume is <u>not</u> constant, we are generally in the limit that $D_{exh} << L_{tot}$, so the variation is small. Therefore, as long as the ambient extinction is much less than the plume extinction, the variation in the background extinction will be small.

This does not mean that background extinction should be ignored: diluted plumes from previous vehicles may cause variations in the background extinction from one vehicle plume to the next, so it is important to monitor the background extinction present for each vehicle. Variations in the background concentrations should occur on a relatively long time scale compared to the plume measurement, so the background extinction can be taken into account by recording the signal just prior to the plume. In order to account for possible variations in the ambient extinction from one vehicle to the next, we form the ratio of the transmitted signals before and after the plume. Because extinction caused by ambient particles simply causes an additional fractional decrease in the transmitted intensity, the ratio of the transmitted signals before and within the plume is independent of the background extinction (neglecting variations in the integrated concentration-pathlength product of the ambient fluid):

$$\frac{I_{plume+amb}}{I_{amb}} = \frac{I_0 \exp\left[-A_{ext,p} M_p L_p\right] \exp\left[-A_{ext,a} M_a L_a\right]}{I_0 \exp\left[-A_{ext,a} M_a L_a\right]}$$

$$= \exp\left[-A_{ext,p} M_p L_p\right] . \qquad (2.3)$$

Another consequence of taking the ratio of the signals with and without the plume is that any slow drifts in the illumination intensity, detector response, or amplifier gain drop out. In other words, the same plume absorber thickness reduces the transmitted signal by the same fraction regardless of the signal level prior to the plume.

Because a ratio is taken, the change in signal caused by the plume mass concentration must be significant compared to noise on the signal with or without the plume. This can be seen if we assume V_1 and V_2 represent the signals before and within the plume, with rms noise levels of σ_1 and σ_2. Analysis of the propagation of the errors [Young, 1962] then leads to

$$\left(\frac{\sigma_Q}{Q}\right)^2 = \left(\frac{\sigma_1}{V_1}\right)^2 + \left(\frac{\sigma_2}{V_2}\right)^2, \tag{2.4}$$

where σ_Q represents the standard deviation of the quotient $Q=V_2 / V_1$. Equation (2.4) can be simplified for the case of $\sigma_1 = \sigma_2 = \sigma_{rms}$ to $(\sigma_Q / Q)^2 = (1 + Q^2)\,(\sigma_{rms} / V_2)^2$. Note that the fractional standard deviation of the quotient has increased by the factor $(1 + Q^2)^{1/2}$ over the fractional standard deviation of the V_2 signal. Since both the soot and CO_2 concentrations are calculated from ratios in this manner, the noise on both signals determine the accuracy of the computed emissions index.

Typical ambient particle concentrations range from $0.020 < M_a < 0.1$ mg/m^3 [Novakov, 1982; Hinds, 1985], but they are not comprised entirely of soot particles. In fact, they are often bimodal, with mass median diameters of the two modes near 0.5 μm and 20-50 μm. The larger mode varies significantly depending on the wind velocity and the height at which the aerosol is sampled. Effective refractive indices for urban particle distributions have been reported as $1.50 + i0.01$ [Hänel, 1988]. The imaginary component typically varies between 0.005-0.02 depending on the average carbon content of the aerosol. This causes the extinction coefficient to vary as well. Hence, slightly higher extinction may occur near roadways which carry a significant number of diesel vehicles. A typical extinction coefficient for relatively dry atmospheric aerosols at λ=630 nm is about 4.2 m^2/g. Periods of high relative humidity which cause condensation or adsorption

processes to occur will increase the ambient extinction significantly. This is yet another reason to monitor the ambient extinction.

For two passes across a single lane (20' between source and reflector, L_{tot}=12.2 m), the typical extinction for M_a = 0.1 mg/m^3 would be about 0.5%. Variations in this value before and within the plume should be less than $2D_{exh} / L_{tot}$, so the variations in the ambient extinction would be on the order of $8x10^{-3}$ for D_{exh} = 4 inches (0.1 m). Hence, as long as the extinction from the ambient aerosol is essentially constant over the time required to make the plume measurement, then we will be able to correct for the background extinction without worrying about the ability to detect 1% extinctions from the plume. Ambient extinction would be important if the path length was long enough such that the transmitted signals became very small.

Ambient CO_2 concentrations are on the order of 350 ppm, *i.e.* 0.035% by volume or 0.053% by mass. For standard atmospheric air (T = 70 °F = 294 K, M_w = 28.97 g/gmol), this implies a mass concentration of 0.64 g/m^3. The only difference between the CO_2 in the plume and the CO_2 in the air is a slight temperature difference. The band absorption coefficient is only slightly affected by temperature, so to first order, we can assume the mass specific absorption coefficient for the ambient CO_2 is also $9.6x10^{-3}$ m^2/g. Thus, the background extinction caused by ambient CO_2 in a double pass across a single lane (L = 12.2 m) would be about 7.5%. Since the extinction by the atmospheric particulates will decrease roughly with $1/\lambda$, extinction by atmospheric particulates should be negligible at 4.2 μm. Variations in this level of background extinction should be on the order of 0.1%; this would not yet cause accuracy difficulties at the 1% level, but significantly longer path lengths could create problems.

To summarize, the range of extinction levels for soot for a double pass through typical exhaust plumes provides adequate sensitivity and dynamic range at the wavelength (630 nm) which is least sensitive to size distribution variations. The same double pass arrangement also provides adequate sensitivity for measuring exhaust plume CO_2 concentrations. In both cases, the extinction caused by particulates and CO_2 in the ambient air is not so large as to preclude accurate measurements of the plume

concentrations. The fact that all four extinction levels fall within these ranges for path lengths which would be typical of a remote sensing measurements is somewhat of an amazing coincidence.

2.5 MEASUREMENT TIME SCALES

An important consideration in the preceding discussion was the time scale over which the measurements must be made. This not only affects our ability to use signal processing techniques such as phase sensitive detection or signal averaging to enhance the signal to noise ratio, but also the assumption that the plume and background extinctions will be constant. The time scale is set by the time required for a plume moving with a vehicle to cross the beam path. The worst case will be when the beam is located right at the exit of a vertical exhaust pipe, such that the time required for the plume to cut across a beam of negligible size is just

$$\Delta t = \frac{D_e}{V_{veh}} . \tag{2.5}$$

This corresponds to about 3.7 ms for a vehicle moving at 60 mph with a 4 inch vertical stack diameter. On the one hand, it is not likely that the ambient concentrations would change on this time scale; however, since typical mechanical choppers used to modulate the light from the incandescent source have maximum chopping frequencies of about 4 kHz, we might only be able to average about 4 pulses or so to obtain better signal to noise levels. Similarly, the bandpass of lock-in amplifiers would have to be set quite large in order to obtain such short time constants, and hence they would also not be very effective. If we allow for some dilution to obtain longer measurement times to enable better signal processing, then the decreased extinction could offset the lower signal noise. Hence, in order to obtain good sensitivity and longer measurement times, one would have to allow for some dilution but use more passes. The limit to which this can be done will depend on the distance across the roadway and the ambient extinction levels.

3.0 EXPERIMENTAL APPARATUS

The primary goal of phase I of the project was to test the validity of the theory just presented under practical conditions. To do this, we had to assemble the components for the remote sensing device, build a gas absorption cell for calibrating the CO_2 response, characterize the emissions of particulates and CO_2 from an engine with accepted techniques, and compare these measurements with those from the remote sensing system. The subassemblies are described below.

3.1 REMOTE SENSING DEVICE

A schematic showing all major components of the remote sensing device is shown in Figure 3.1. Each component will be discussed in detail such that the correspondence between the theory and the experiment are clear. Suggestions for modifications appear in the recommendations in Chapter 6.

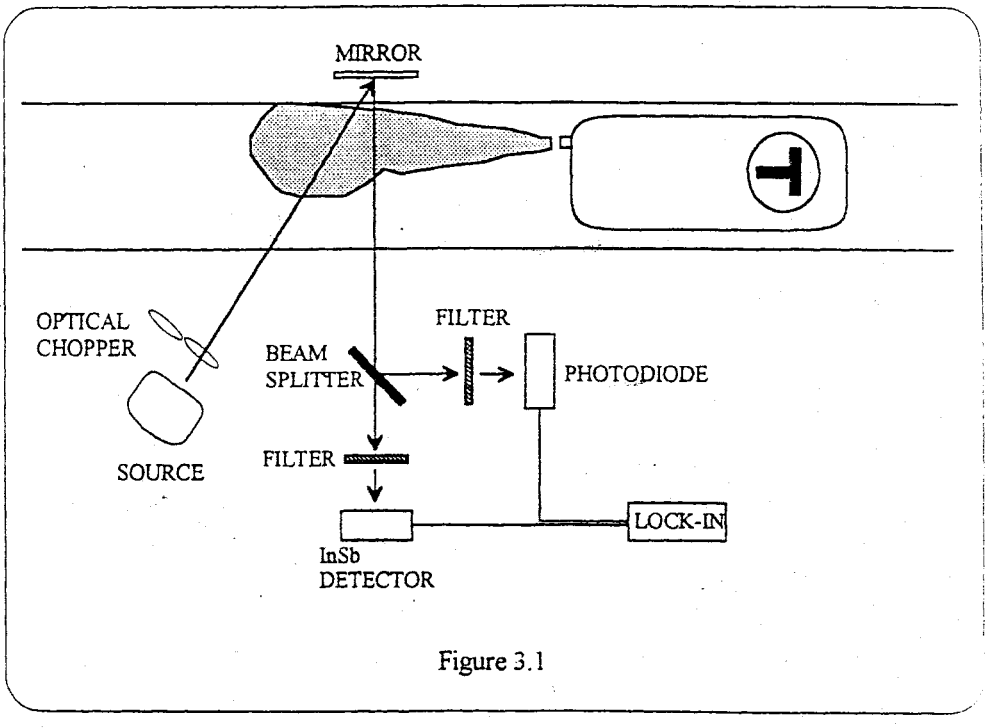

Figure 3.1

Fig. 3.1: Schematic of remote sensing apparatus.

3.1.1 Source

As mentioned in section 2.3, the ν_3 band of CO_2 is centered at 4.26 . Thus, the source must emit in the infrared region surrounding 4.26 μm. Particulates also absorb and scatter light at this wavelength, but far less than they do at shorter wavelengths; therefore, using a shorter wavelength to detect particulates will increase detection sensitivity. An incandescent source emits relatively intense broadband radiation from the visible through mid-infrared regions, and hence can supply sufficient optical power for detecting both CO_2 and particulates. Using a single source also simplifies alignment, since it eliminates the need to overlap the beam paths of two separate sources, which is required if the ratio is to be computed independent of plume dilution. The simplest and most cost-effective solution was found to be a 50 watt quartz tungsten-halogen lamp (Gilway Technical Lamp); the filament dimensions of this lamp were 5.6 x 1.6 mm.

3.1.2 CO_2 Detector

A number of infrared detectors are sensitive to ν_3 of CO_2 (4.2-4.3 μm). An InSb (indium antimonide) detector (Model J10D, EG&G Judsen) was chosen because it has the highest detectivity (D*, the signal-to-noise ratio (S/N) for a given size, chopping frequency and frequency bandwidth) at this wavelength. The detector is cooled by thermal contact with a liquid nitrogen (LN_2) dewar; this reduces the dark current, and hence noise, from the detector. The active diameter was only 2 mm, which limits the allowable level of vibration in the source and collection optics. This will be discussed in more detail in section 3.1.5.

InSb detectors are sensitive from about 1 to 5.5 μm. Since the source emits light throughout this range, a filter is necessary to ensure that only light within the ν_3 band of CO_2 affects the signal. An interference filter with a center wavelength of 4.269 μm, full-width half-maximum (FWHM) of 90 nm, and peak transmission of 88% (OCLI) was used. The filter is housed in the dewar attachment directly in front of the detector, and cooled by means of a cold finger in thermal contact with the LN_2. This maintains the filter

temperature at a constant value, which is important because the bandpass of interference filters is somewhat dependent on temperature.

3.1.3 Particulate Detector

A silicon PIN photodiode (Hamamatsu) detected absorption due to soot. The wavelength response extends from about 320 to 1060 nm, with a peak near 700 nm. These diodes have relatively fast response and good linearity when reverse biased, and are also relatively inexpensive. The model chosen had a 2.54 mm active diameter such that the volume viewed by the photodiode would be essentially identical to the volume viewed by the InSb infrared detector. A Schott KG3 heat absorbing filter was placed in front of the photodiode to reduce sensitivity to water bands in the near infrared. The KG3 filter is a short pass filter with a 50 % transmission at 700 nm, about 10 % by 825 nm and only around 1 % by 925 nm, but it does not attenuate shorter wavelengths until below about 350 nm.

In retrospect, we should have employed a bandpass filter centered at about 650 nm with a FWHM of about 50 nm. This width should be sufficient to ensure the transmitted light is detectable, yet it would also limit the range over which the soot absorption measurement occurs. The reason for such a bandpass restriction was discussed in the theory; without one, the response characteristic of the soot channel is not truly exponential. However, because the rate of change of the combined detector response and short pass filter is quite slow and peaks near 650 nm, the average extinction coefficient over the entire spectrum turns out to be similar to that near 630 nm (*i.e.*11m^2/g).

3.1.4 Optical Chopper

The source was modulated by an optical chopper (Stanford Research Systems). Source modulation in conjunction with detector signal demodulation allows detection of small signals in the presence of a large background. For example, background sunlight will be visible to both the photodiode and the InSb detectors, but only the light from the source will be modulated at the chopping frequency, f. Thus, if only changes in the signal

amplitude which fall within a narrow band about f are recorded, one can discriminate quite effectively against background radiation and noise from the detectors and amplifiers, since they will not be at the same frequency.

Because the calibration experiments are conducted at steady state operating conditions, one could consider using a lock-in amplifier. However, two channels must be simultaneously processed and recorded, which would require an expensive two channel system. Moreover, if the signal fluctuates with time, for example because of pulsating flow from the engine, then the lock-in passband must be wide enough to ensure that the output signal can respond fast enough to record the fluctuations. Alternatively, the entire signal can be digitized and recorded, and then post-processed using Fourier transform techniques to identify the strength of various frequency components in the signal. The latter method has the advantage of helping to identify other processes which affect the signal, and was used in the engine tests presented here.

3.1.5 Optics

The remote sensor requires three additional optical components: 1) a collimating mirror, 2) a plane reflecting mirror, and 3) a beamsplitter. The purpose of the collimator is to collect light from the source and form a collimated beam for transmission across the road. The plane mirror reflects the beam back across the road, such that both source and detectors can easily be powered from a nearby generator. This also doubles the path length through the plume to obtain better sensitivity at low concentrations. The beamsplitter splits the energy in the beam and sends it to the two different detectors, allowing both CO_2 and soot to be monitored simultaneously.

An off-axis segment cut from a 6.87 inch focal length rhodium-coated nickel parabolic reflector (Optical Radiation Corp.) served as the collimating mirror. A mirror is used rather than a lens because reflection is achromatic, which implies the mirror will collimate both visible and infrared wavelengths equally well. The relatively long focal length allows ample room to position the chopper between the source and the mirror. The plane mirror (Oriel) was 8" in diameter to ensure easy alignment, and had a front-coated

aluminum silicon monoxide surface appropriate for outdoor use. The beamsplitter was a simple silicon wafer (donated by Pure Sil, Inc.). Silicon reflects visible radiation and transmits infrared radiation with a flat response between 1-6 μm.

A difficulty in optical imaging arises from using an extended source. Since the source is not a point source, the parabolic mirror will not create a perfectly collimated beam. Thus additional light will be lost since some of the light will be diverging. Most of the light which reaches the detectors, however, should be fairly well collimated.

The collimated beam could be refocused onto the detectors by a second parabolic reflector to achieve a greater signal. However, slight vibrations of the optical components due to passing traffic could be enough to cause the focal point to fall completely or partially off the detectors, resulting in false extinction signals. For this reason, the beam is not refocused. Since the size of the collimated beam is much larger than the active area of the detectors, small vibrations should not affect the measured signal.

3.1.6 Amplifiers

The output of the each detector passes through a single stage low-noise preamplifier to boost signal strength. The InSb signal enters an EG&G Judsen PA7-60 preamp with selectable gain of 2.5×10^4, 10^5, and 10^6 V/A. The photodiode signal enters a transimpedance amplifier with a conversion factor of 10^6 V/A. These amplification values are necessary in order to bring the signal voltages into the proper range for the data acquisition board.

3.1.7 Ambient CO_2 Analyzer

A Beckman model IR215 infrared CO_2 analyzer was used to measure the ambient CO_2 concentration, both in the absorption cell experiments and in the engine tests. The ambient concentration - pathlength product must be known in each case, because the calibration curve for the CO_2 response is not purely exponential. Unfortunately, the Beckman analyzer was prone to drift, making an accurate determination of the ambient CO_2 concentration very tedious. This would be unacceptable for an on-road

measurement, where ambient conditions might change fairly quickly and quite often due to changing wind and traffic conditions. State-of-the-art instruments of this sort cost in the neighborhood of $10,000 new.

3.2 ABSORPTION CELL

The instrument response for the CO_2 channel was calibrated using a laboratory absorption cell. A White-type absorption cell was constructed for this purpose, allowing the optical pathlength to be set to a number of discrete steps between 4 and 100 meters [White 1942]. Such cells are commonly used to measure the absorption from gases over a range of concentrations and pathlengths. In this case, we filled the cell with gas mixture which had known concentrations of CO_2, and measured the resulting signal over a known pathlength. As the CO_2 concentration increased, the absorption increased, and hence the signal decayed. A plot of the response provides the calibration curve described in the theory, and is given in the next chapter.

3.3 ENGINE AND DYNAMOMETER

Preliminary tests of the remote sensing system were carried out on a Caterpillar 3304 naturally-aspirated indirect-injection (IDI) diesel engine. This is a 4 cylinder, 7 liter displacement engine with a maximum rating of 100 horsepower at 2200 RPM. The fuel equivalence ratio (i.e. engine load) was controlled by a pneumatic actuator linked to the fuel injector rack. The engine was connected to a General Electric DC dynamometer to absorb power. Small engine torque and RPM fluctuations could occur due to limitations associated with the fuel supply and dynamometer control systems, but they should not have been significant over the duration of the measurements.

Engine emissions were measured using several instruments. The CO_2 concentration in the engine exhaust was monitored with a Horiba PIR-2000 CO_2 analyzer. This is a state-of-the-art non-dispersive infrared analyzer designed specifically for measuring engine emissions. A mini-dilution tunnel apparatus was constructed for the purpose of measuring the volume concentration of the soot in the exhaust [Kittelson *et al.*,

1994]. This apparatus dilutes the exhaust flow by a factor large enough that the soot concentration can be accurately measured with an Electric Aerosol Analyzer. The dilution ratio of the tunnel is measured on line by monitoring the NO_x concentrations upstream and downstream of the dilution air. Before entering the EAA, the flow could be passed through a catalytic heater or diverted through a bypass around the heater. The purpose of the heater is to oxidize the volatile fraction of the particulate mass; in this way, measurements of both the total particle volume concentration and the nonvolatile particle volume concentration could be made by alternately using or bypassing the heater. The bypass could be selected rapidly with the use of several valves such that the total and nonvolatile measurements could be performed in fairly rapid succession. Significant effort was required to assemble and verify the operation of the tunnel.

A Bosch Smoke Meter was also used to sample the exhaust from the exhaust manifold to obtain qualitative indications of the soot concentrations as corroborating evidence for the EAA measurement. It is well known that such smoke meter measurements are not quantitatively accurate with regard to mass concentrations, but they do provide a qualitative indication of soot emission levels which are fairly reproducible for a given engine operating under known speed and load conditions.

4.0 PROCEDURE

4.1 CO_2 CALIBRATION WITH ABSORPTION CELL

The instrument response to CO_2 concentrations was calibrated in the laboratory with an absorption cell. The detailed procedure can be found in T. J. Prochnau's master's thesis [Prochnau, 1994]. Different absorber thicknesses of CO_2 were obtained by mixing varying amounts of a span gas of 0.98% CO_2 in air (21.1% O_2 and 77.9% N_2) with zero air (a reference gas of CO_2-free air). The concentration of the CO_2 in the resulting mixture was thus controlled by the amount of span gas that was added. A small fan inside the absorption cell mixed the gases for several minutes before any measurements were performed to ensure uniform concentrations when data was acquired.

A reference value of $\rho_{CO2}L$ was chosen as 71.4 g/m^2, the condition where the absorption cell was filled completely to atmospheric pressure with the CO_2 span gas and the path length of L = 4 m was used. This absorber thickness was selected for four reasons. First, no mixing of cylinder gases was required and thus the uncertainty in the CO_2 concentration was reduced. Second, the signal voltage is less sensitive at higher $\rho_{CO2}L$ and so will have less variability with small changes in $\rho_{CO2}L$. Third, part of the path between source and detector occurred within the room air, and we wanted to ensure that uncertainties in the contribution of the room air absorber thickness were small compared to the reference value. The ambient path length was 2.35 ± 0.04 m , and the ambient concentration was generally about 350 ppm, giving an ambient absorption thickness of about 1.5 g/m^2. Since the uncertainty in the ambient CO_2 instrument was only about ±3%; the total uncertainty in the ambient absorber thickness was not significant when compared to the reference value. All of these uncertainties would have become more important had the reference signal been chosen as zero air plus the ambient air absorption. Finally, the maximum CO_2 absorber thickness expected is of the order (100 g/m^3)(0.2 m) = 20 g/m^2, so the calibration will cover the expected range of the measurements.

The cell was filled with various mixtures of span gas and zero air in order to obtain a range of CO_2 concentrations. Accurate measurements of V_{sig} and V_{ref} were obtained by modulating the light source at 400 Hz and using a lock-in amplifier to maximize the signal-to-noise ratio. 30-second scans were taken with a 30 ms time constant (2.6 Hz bandwidth with 24 dB/octave filter rolloff). The time constant was selected following two criteria. First, it had to be long enough that the chopper could modulate the signal at least a few times during each time constant in order to obtain a lock (in this case 12 cycles per time constant). Second, it had to be short enough so that it would be representative of filtering techniques which might be employed in on-road measurements. Trace scans were taken simultaneously for the signal, signal noise, ambient CO_2 concentration, and ambient temperature for each measurement, and the average and standard deviation was calculated for each scan.

4.2 INITIAL TESTS ON ENGINE EXHAUST

Initial tests were performed on the exhaust emitted from the Caterpillar engine to ascertain whether the technique gave reasonable results. The remote sensing apparatus was set up on the roof of the Mechanical Engineering building as shown in Figure 4.1, with the engine exhaust emitted from a 3" horizontal pipe. The source modulation frequency was set using the chopper at 400 Hz. The soot and CO_2 transmission signals were sampled simultaneously at a rate of 4 kHz with 12 bit resolution. This gives a theoretical ability to record frequencies up to 2 kHz, would should enable very accurate recording of the primary 400 Hz signal.

A collimated beam with a diameter of one inch was directed through the center of the plume approximately 12" from where the optical beam intercepted the plume. This was done so that the plume would have some opportunity to disperse and mix with the surrounding air to simulate the plume dilution of a moving vehicle. The plume boundary was estimated to have spread to a diameter of about 9" at the point of intersection with the optical beam. The beam was centered on the detectors, but not refocused.

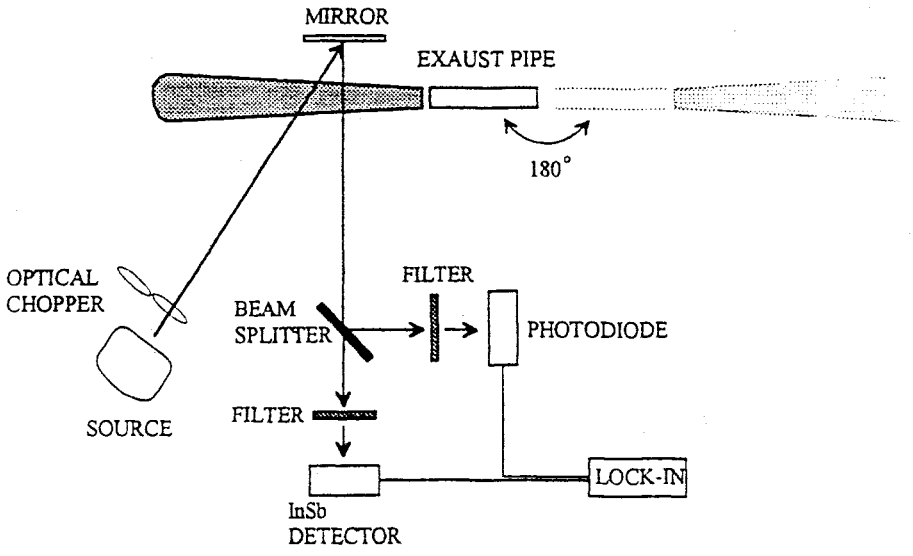

Fig. 4.1: Schematic layout of engine exhaust extinction measurements.

The Horiba CO_2 analyzer sampled the engine exhaust, and the values were recorded for each load condition. The Bosch smoke meter was located near the EAA sampling point, just downstream of the exhaust manifold. (Interested readers should refer to the 1994 Society of Automotive Engineers Handbook for details about the operation of the smoke meter.) The exhaust temperature was also monitored at this point. Again, the Beckman CO_2 analyzer was used to monitor the ambient CO_2 concentration.

The engine was run at low, half, and full loads at speeds of 1200 RPM, 1400 RPM, and 2000 RPM. V_1 and V_2 were measured by the InSb and photodiode receivers, respectively, and sampled at 4 kHz (10 times the chopping frequency). Several 1 second long records were taken at each operating condition. The exhaust pipe exit direction was rotated 180° to toggle between ambient and plume measurements. A time delay of about 2 minutes was used between the plume measurements and the ambient measurements to ensure that residual plume concentrations had been allowed to disperse.

5.0 RESULTS AND ANALYSIS

5.1 CO_2 CALIBRATION WITH ABSORPTION CELL

Data was taken following the procedure outlined in section 4.1. Seven values of $\rho_{co2}L$ were chosen within the range of CO_2 absorber thicknesses which would be expected in a double pass through a 10 cm exhaust plume (see sections 2.3-2.4). Initial tests were conducted to acquire fourteen data points on four different days. Figure 5.1 compares the measured data to the theoretical extinction predicted by a computer model which employed incorporated equation (B.28) together with known spectroscopic data [I rochnau, 1994].

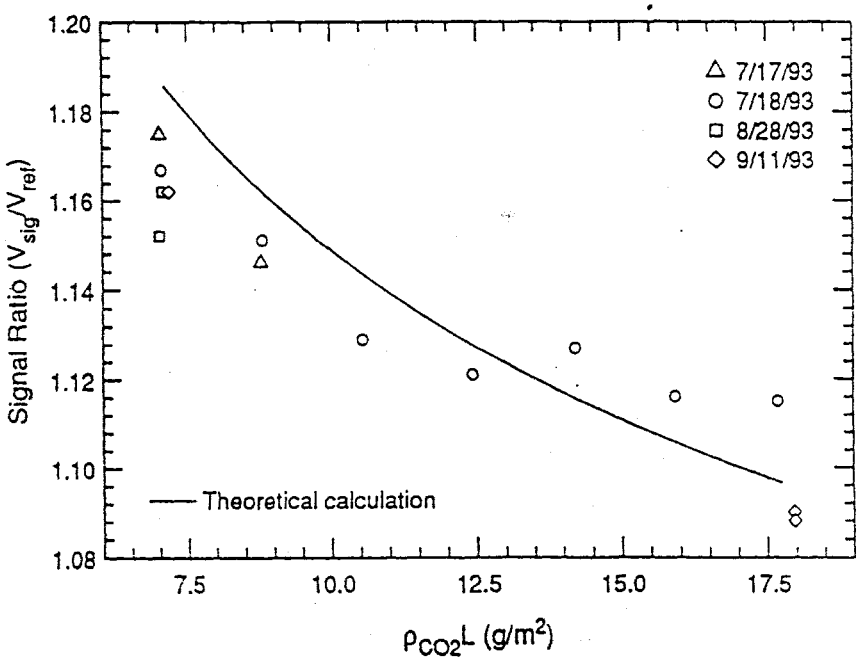

Figure 5.1. Measured data and theoretical calculations for InSb detector signal ratio versus $\rho_{co2}L$. Reference value is at $\rho_{co2}L$=71.4 g/m^2.

As seen in this figure, the theory appears to overpredict the measured signal ratio (the three high points on 7/18/93 will be discussed below). The cause of the difference was attributed to the transmission function assumed for the bandpass filter in front of the InSb detector. The relative spectral response of the filter transmission times the detector

responsivity was measured by EG&G and plotted on a linear (rather than logarithmic) transmission scale. On this scale, the filter transmission appears to drop to zero approximately twice the FWHM away from band center; the computer model digitized this profile and assumed zero transmission at all other wavelengths. However, it is not unusual for filters of this type to transmit 0.01-0.1% in spectral regions far from band center. Since light from a broadband source is incident on the filter, a background signal will be present which is not sensitive to CO_2 concentrations. Thus both V_{sig} and V_{ref} would be greater and the signal ratio would be smaller (closer to unity).

To account for this out-of-band transmission, the model was altered to allow filter transmission across the entire spectral range of the detector response. The best fit to the data occurred assuming a filter transmission of 0.02%. Figure 5.2 shows the predicted response neglecting the three highest $\rho_{CO2}L$ values taken on 7/18/93, along with bounding curves defining $\pm 1\sigma$ from the curve for this small data set. The agreement is quite good.

The error bars shown in Fig. 5.2 represent the uncertainty in the true absorber thickness present in the absorption cell and were estimated as follows. The uncertainty in measuring $\rho_{CO2}L$ was conservatively estimated by assuming uncertainties of 1 cm for the absorption cell pathlength, 4 cm for the external pathlength, 2 Torr for the span gas inside the cell, and about 3% for the ambient CO_2 monitor. The total estimated uncertainty in $\rho_{CO2}L$ ranges from 0.27-0.30 g/m^2. The uncertainty in measuring L is a systematic error, since the actual pathlength does not change with separate measurements; without including the systematic error, the estimated uncertainty ranges from 0.235-0.240 g/m^2. The uncertainty in the signal ratio due to variations in $\rho_{CO2}L$ can be calculated from the slope of the line; the signal uncertainty ranges from 0.0014-0.0037 over the range shown.

The standard deviation for the five data points taken at the lowest absorber thickness (where the slope of the signal ratio line there is the greatest) was 0.0076, lower than the value of 0.0091 calculated from the least square residual found between all 11 points and the best fit theoretical curve. The lowest absorber thickness was chosen because the higher slope implies that the change in signal ratio due to a small change in

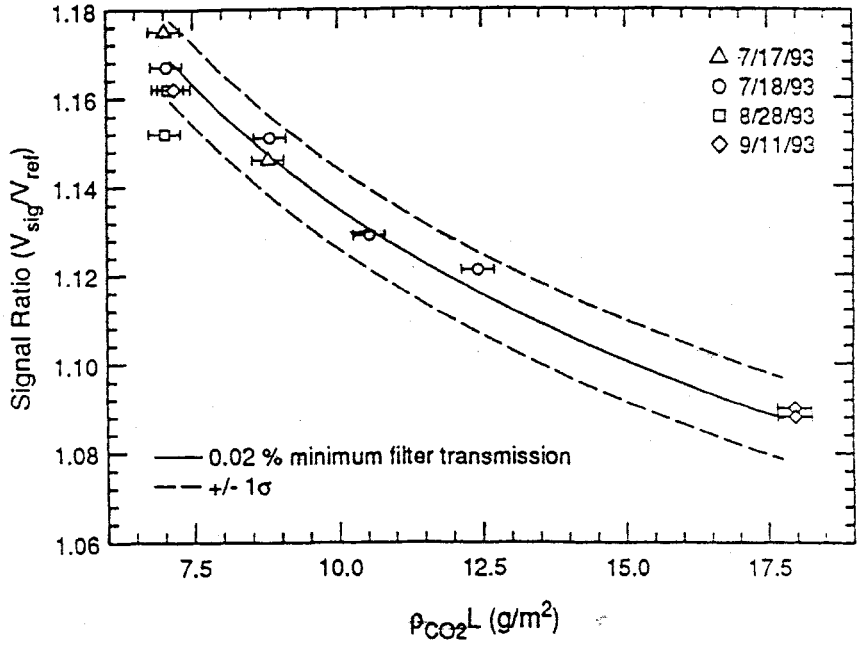

Figure 5.2: Fit of 11 data points to theoretical calculation with 0.02% minimum filter transmission for InSb detector signal ratio versus $\rho_{CO2}L$. Dashed lines show +/- 1σ from curve, with σ=0.0091, while error bars represent uncertainty in absorption cell concentrations. The reference value is at $\rho_{CO2}L$=71.4 g/m^2.

$\rho_{CO2}L$ is the greatest. Thus the size of the error bars should be a conservative indication of the uncertainty at all values of $\rho_{CO2}L$. The fact that the data points show a larger deviation from the theoretically predicted curve than would be expected based on our estimate of uncertainties could indicate that our theoretical model is not completely accurate, or that more data points must be taken to overcome the uncertainty in $\rho_{CO2}L$ in the absorption cell.

As for the three errant points, the apparent systematic error was initially attributed to high humidity. During the time when several measurements were taken, the weather changed rapidly from clear to thunderstorms to clear again; presumably the humidity also increased and decreased. Assuming the humidity changed on a time scale slower than the time required to measure both V_{sig} and V_{ref}, the numerous water bands that occur in the

out-of-band spectral region would effectively reduce the background level on both signals, thereby increasing the signal ratio.

This hypothesis was tested by simulating water absorption over the spectral range of the detector. A worst-case scenario was modeled by identifying the strongest water bands [from Howard 1965] and assuming zero transmission throughout these bands. As expected, the predicted curve is shifted up slightly, but the amount is not great enough to account for the three questionable data points. Moreover, the assumption of completely opaque water absorption bands taken over the relatively short path length through the ambient air will overestimate the impact of water vapor on the background.

A second possibility for the three spurious points is a leak in the absorption cell. Since the cell is at sub-atmospheric pressure when being filled, a leak would allow room air into the container, diluting the intended CO_2 concentration. Because the data require two measurements, one for V_{sig} and one for V_{ref}, a leak should affect both CO_2 concentrations. Since V_{sig} is more sensitive than V_{ref} to changes in $\rho_{CO2}L$, one might expect the signal ratio to increase when a leak is present. A final possibility is a systematic error in filling the absorption cell. We have never again been able to reproduce the ratios indicated by the three high points on Fig. 5.1, and hence feel justified in discarding these points as bad data points.

The greatest source of error in measuring the signal ratio is due to drifting over the relatively long time period (15-25 minutes) between the V_{ref} and V_{sig} measurements. The cell cannot be rapidly pumped down and refilled between these measurements because doing so causes the end plates to flex and the optics to misalign. Moreover, the gases must be allowed to mix completely or the signal acquired will not be representative of the average concentration computed from the mixture ratios. The drifting occurs primarily from line voltage fluctuations which cause variations in the source strength. The SOLA constant-voltage transformer helped isolate the more abrupt short-term fluctuations but still allowed some longer-term drift to occur. Another possible source of drifting would be the changing of optical alignment during and after varying the absorption cell pressure; enough time was allowed to pass (at least five minutes) before taking the measurement

that there was no observable alignment drift over the 30-second interval of the trace scan. Amplifier drift, a possible contributor to error often caused by changes in humidity, usually occurs over a longer time span and is thus not likely to be a large factor here.

Source intensity drifting could be corrected by monitoring the source intensity within the CO_2 band before it enters the cell. This would require a second InSb detector and another interference filter. The source intensity in the CO_2 band itself must be monitored rather than the source intensity at some wavelength in the visible because different wavelengths do not undergo the same relative change in intensity if the filament temperature changes. Since a change in source intensity implies that the current to the filament has changed, and hence also the filament temperature, using the visible source intensity to correct for source intensity variations in the CO_2 band would be ill-advised. A second detector and filter system was not available at the time of the measurements; the cost of obtaining one would be about $5000. The additional accuracy may not be necessary, since the remote sensing measurements between ambient and plume must be recorded on a very short time scale.

5.2 INITIAL TESTS ON ENGINE EXHAUST

Initial calibration tests were performed on the Caterpillar 3304 diesel engine in the laboratory following the procedure outlined in section 4.2. Bosch smoke numbers were converted to total soot mass concentrations using data available in the 1994 SAE Handbook.

Several difficulties arose in analyzing the collected data. First, turbulent fluctuations in the plume concentrations superimpose a time-varying envelope on the 400 Hz source modulation. This modulation shows up on both the CO_2 and the soot channels as one would expect (see Fig. 5.3). Unfortunately, there is no such modulation in the data collected without a plume present. Hence, one cannot simply take the ratio of the amplitudes of the signals with and without the plume in order to compute the extinction; the data must first be filtered if one is to estimate the extinction caused by the soot or CO_2 species individually. This does not mean that information in the time variation

of the signals should be discarded by filtering the incoming electrical signals before they are digitized. In fact, the frequency variations recorded in the plume signals even indicated the presence of a low amplitude variation at the frequency of individual cylinder exhaust events! This small variation remains at the exhaust pipe exit even after passing through the engine exhaust surge tank which is designed to damp out the flow pulsations caused by individual exhaust strokes, and the long stack which extends through the roof.

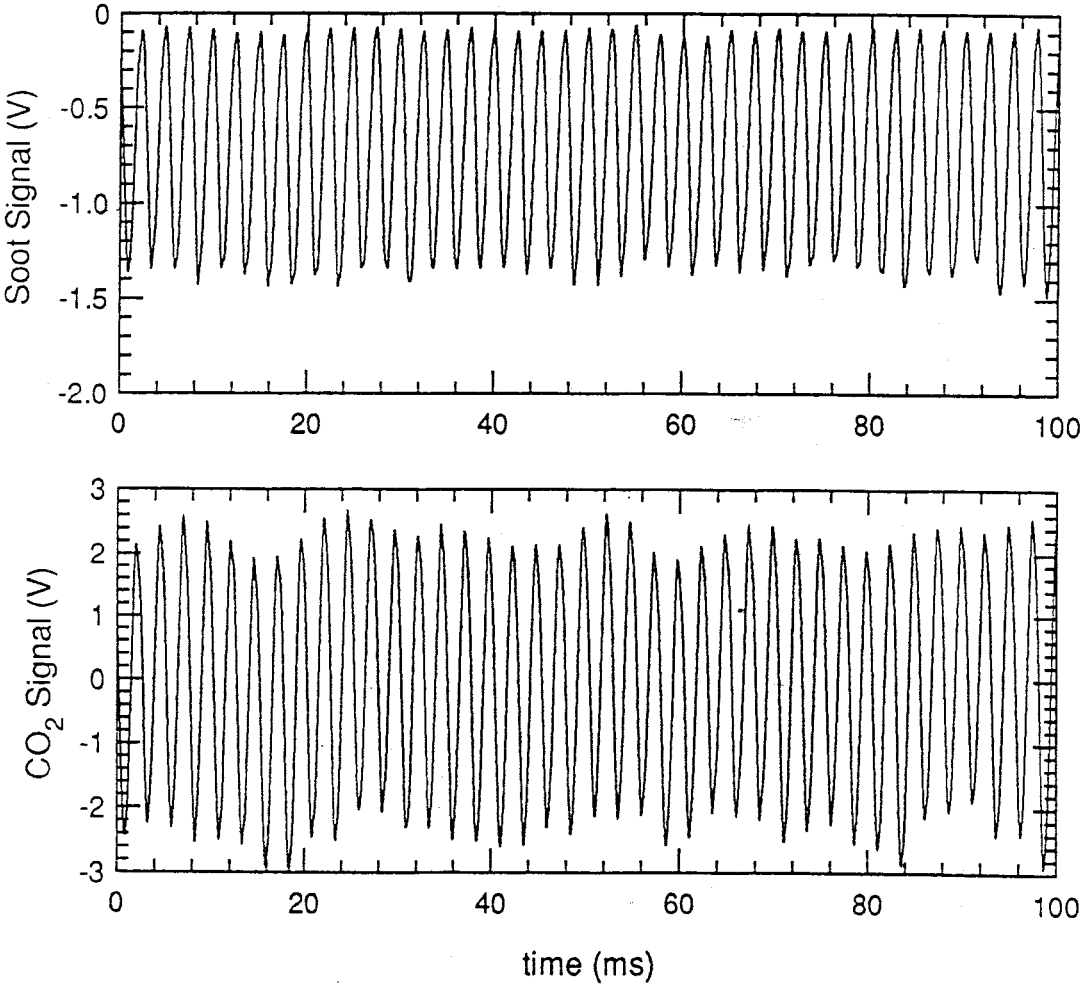

Fig. 5.3: Unprocessed signal for the soot and CO_2 channels through an exhaust plume under full load conditions. The primary frequency is that of the chopper, 400 Hz. The envelope modulations are caused by turbulent fluctuations in the plume.

These variations occur in both the CO_2 and soot signals, and hence do not affect the ratio between the CO_2 and soot concentrations as long as both signals remain in phase with one another; however, they do affect the ability to determine the extinction due to soot or CO_2 concentrations individually, because the absolute amplitude is affected. This is exactly the problem that was described in Chapter 2, and the reason that a ratio is required. The average amplitude of the of the 400 Hz signal can be filtered out of the signal using conventional Fourier transform techniques. This could also be done using bandpass filter circuits to process the signal before it was digitized. However, the latter method eliminates our ability to see the total temporal and frequency dependence of the signal, which is useful for identifying noise sources or other sources of signal structure (*e.g.* 60 Hz noise on the amplifiers or individual cylinder exhaust events).

The ratio between the average amplitude through the plume and the average amplitude through the ambient for the soot and CO_2 channels allows us to estimate the average soot and CO_2 concentrations through the plume by estimating an effective path length. These numbers can then be compared to the values measured by the EAA and CO_2 analyzers, which sample the engine exhaust directly. Because the exhaust plume has already undergone a small amount of dilution at the point it was measured, there is some uncertainty in the effective path length - concentration product.

In addition, there is a significant time delay between when the plume measurements are recorded and when the ambient background measurements are recorded. This results from the need to reposition the exhaust pipe outlet. Any drifts in amplifier gain or source intensity during this time period will affect the values of the concentrations inferred from the extinction measurements. In fact, such drifts did occur for several of the test cases we measured, since both the soot and CO_2 signals increased when the plume was present. These points were discarded from the data set as unphysical. Such an effect would not occur in true on-road measurements because the ambient and plume measurements would be recorded within very short time intervals of one another. Thus, we do not expect the extinction and sampling measurements to agree exactly, but we can at least determine if they are on the proper order of magnitude. However, the ratios between the soot and CO_2

concentrations as measured by the extinction and sampling methods should agree if the extinction technique works well.

The results of the initial engine experiments are summarized in Fig. 5.4 on the following page. The two upper curves, Fig. 5.4 (a) and (b), compare the average plume concentrations estimated from the extinction measurements with those measured by the EAA and the Bosch smoke meter. The extinction mass concentrations are obtained from measurements with and without the plume using L = 0.14 m and A_{ext} = 11 m^2/g. Zero values of soot were recorded in cases where the soot signal exhibited a slight increase with the plume present. Since negative concentrations of soot are not possible, probable causes include a slight drift in the gain of the soot detector circuit or a change in the source intensity. The former is more likely, since the CO_2 data appeared fine for the cases plotted. The EAA data shown are for the nonvolatile portion of soot particles whose sizes are less than 1 μm. This is obtained by using an impactor to take out particles greater than 1 μm in size (large particles tend to be entrained from the walls of passing the diluted exhaust through a catalytic heater held at 300°C prior to measuring the EAA instrument. The volume concentration obtained from the EAA is converted to a mass concentration assuming an effective density of ρ = 1 g/cm^3. The Bosch data are for the total soot mass concentrations, obtained from the smoke number measurements using an empirical correlation derived from data given in the 1994 SAE Handbook. Hence, one expects the EAA dry soot mass concentrations to be less than the Bosch smoke number total mass concentrations, but neither the EAA-derived concentrations nor the Bosch-derived concentrations would necessarily agree with full-scale dilution tunnel measurements of the corresponding particulate matter mass concentrations. However, the trends recorded by the EAA and the Bosch smoke meter measurements obey similar patterns for most of the operating conditions shown, and hence we feel confident that the numbers are representative of actual concentrations.

The data are for three different engine speeds and three different load conditions. In general, one expects soot concentrations to increase with the amount of fuel injected,

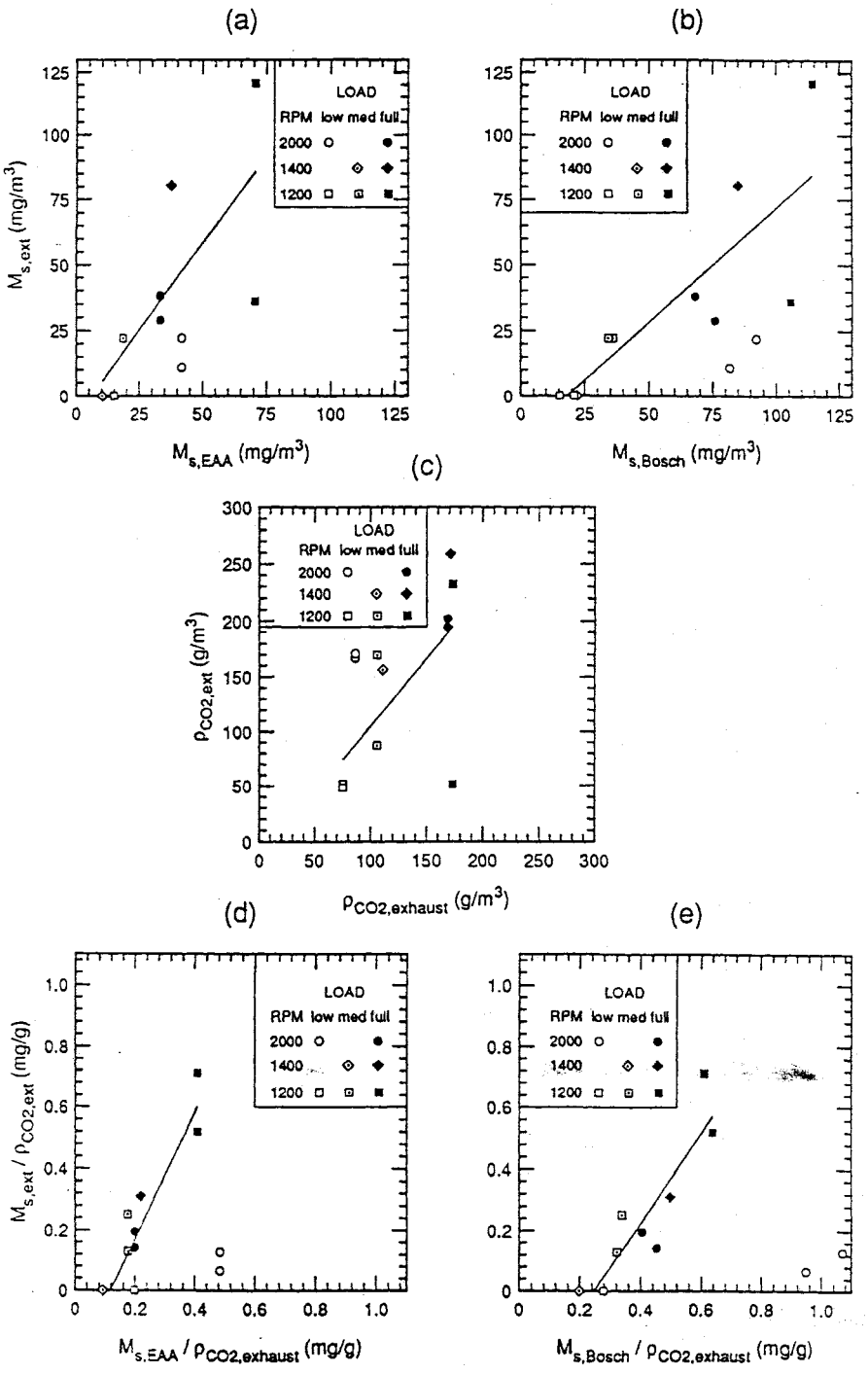

Fig. 5.4: Comparison of extinction and sampling results for Caterpillar 3304 engine under a variety of speeds and loads. (a) and (b) compare average soot mass concentrations determined by extinction to those obtained by EAA and Bosch instruments, respectively; (c) compares CO_2 density to that measured by the Horiba exhaust gas analyzer. The large variabilities in (a-c) result from turbulent fluctuations in the plume. (d) and (e) compare emission index ratios corresponding to (a) and (b). A best fit line with no weighting is shown in all plots, excluding the two points at 2000 rpm and light load (see text).

i.e. with engine load. The 2000 rpm case actually goes in the opposite direction according to both the EAA and Bosch measurements; this must be caused by a change in the turbulence characteristics associated with the flow from the pre-chamber to the main chamber at high speeds. The large spread in the concentrations measured by the extinction technique is to be expected because the instantaneous path length - mass concentration product through the plume varies due to dilution and wafting of the exhaust plume. This is why it is not wise to calculating absolute concentrations from the extinction measurements; our purpose here is to show that on the average, the results obtained by doing so agree fairly well with expectations. If the extinction measurements scaled with increasing soot concentration in the same way as either sampling measurement, the best fit lines shown would have a 45° slope. The extinction measurements appear to scale more like the total mass concentration as determined from the Bosch smoke number but with magnitudes more indicative of the nonvolatile EAA values. We should point out that the relative magnitude could be increased by reducing the effective path length, but this does not seem justified based on observations of the plume divergence during the experiment.

The CO_2 concentrations shown in Fig. 5.4(c) must be obtained in several steps. The signal ratios must first be corrected for the small amount of extinction at 4.2 μm caused by the presence of the soot. The correction was done using the soot concentration measured by the extinction method and assuming a size-averaged extinction coefficient of 1.3 m^2/g at $\lambda = 4.2$ μm (computed from Lorenz-Mie theory, see Fig. B.1). The correction is necessary or absorption by soot will increase the apparent CO_2 concentration for the extinction measurements. Next, the CO_2 concentration must be calculated iteratively since the absorption cross section is not independent of concentration. The first estimate is calculated assuming an average absorption cross section of $\beta_{ext} = 0.0096$ m^2/g and the same effective path length as was used for the soot computations, L = 0.14 m. From this estimate, a new absorber thickness can be calculated, and a more accurate value of β_{ext} can be read from the CO_2 calibration curve. For cases which fall outside the calibration range,

the value corresponding to β_{ext} for the nearest measured data was assumed. This procedure converges quite rapidly to the final value of ρ_{CO2}.

With the assumed value of the path length, the CO_2 concentrations appear to be overpredicted by the extinction measurements. This could be explained if L were adjusted to a longer pathlength, or due to a slightly higher value of the absorption coefficient in the engine experiments. Without correcting for variable β_{ext}, the slope of the correlation line is less than 45°; with the correction, it is slightly greater than 45°. The soot correction could be the source of the problem, but most likely the error lies in a difference between the calibration response curve and the engine measurements, such as might be caused by differences in the filter response. The calibration experiment needs to be repeated to increase the calibrated range and check the sensitivity to alignment variations.

Figures 5.4(d) and (e) plot the ratio of the soot to CO_2 concentrations shown in Figs. 5.4 (a-c). Since the ratio is theoretically independent of dilution and pathlength, then it should give results which compare well with the sampled results. Although the slope of the extinction measurements is higher in both cases, the large variance indicated in Figs. 5.4 (a-c) has been greatly reduced. This confirms the theory of taking ratios.

The results confirm our expectations that the low speed, high load conditions produce the most soot per unit mass of fuel burned. The higher than expected sensitivity to soot indicated by the slopes of the lines is not necessarily real, as the fit might be significantly different if the artificially assumed zero soot concentration points for the extinction measurements were deleted. To confirm this, we would have to reduce drift in the detectors and build a bypass exhaust pipe such that the background and plume measurements could be taken in rapid sequence. The two results obtained for 2000 rpm and low load do not agree with the other cases; referring to the preceding figures, the soot was underpredicted by the extinction technique while the CO_2 was overpredicted. We do not have a good explanation for this behavior at this time, other than to say that we will repeat the measurement to check for a measurement error.

The ratios shown in Fig. 5.4 can be converted to units of g/bhp-hr by multiplying by the total exhaust flow rate and dividing by the engine power. These are both known for the laboratory engine. We have not done so to avoid the implication that similar results could be readily obtained in the field under any operating condition. Since in a remote measurement, one can only estimate the engine flow rate and the power output of the engine under a given operating condition, a number of measurements would be necessary to obtain reasonable accuracy, or the measurement location would have to be chosen such that the operating condition was fairly well-known. We feel that this overly restricts the usefulness of the remote sensing technique, since its power lies in the ability to identify vehicles which emit particulate levels well above the norm at a particular fuel consumption (*i.e.* above the lines shown in Fig. 5.4 (d) or (e)). The power and flow rate information are not necessary to determine this performance indicator.

The fact that the soot concentration must be known in order to correct the CO_2 concentration presents a limitation in the method. If the visible wavelength extinction measurement overpredicts the soot concentration, the soot extinction in the CO_2 band will also be overpredicted. Hence, the CO_2 measurement will be over-corrected, and the CO_2 concentration will be underpredicted. The opposite would occur if the soot concentration was underpredicted by measurements in the visible region. The effect is not large, because the extinction by soot in the CO_2 band is quite small, and the error introduced in the CO_2 concentration depends only on the difference between the actual soot concentration - extinction cross section product and that calculated from the visible extinction and the assumed infrared soot extinction cross section. In fact, the soot corrections to the CO_2 concentrations were much smaller than the effect caused by using a variable absorption cross section. Still, when the ratio is computed, the errors will be amplified . One could monitor the soot extinction at a wavelength nearer to the CO_2 channel more accurately, say at 3.9 μm. This wavelength would require more passes through the plume to get a reasonable amount of extinction from the soot, as well as another InSb detector; at this time, it is not clear whether the added accuracy would be worth the effort when other sources of uncertainty are considered.

6.0 CONCLUSIONS AND RECOMMENDATIONS

An instrument has been developed and constructed to extend the principles of remote sensing to enable real-time detection of particulate emissions from heavy-duty vehicles under actual roadway operating conditions. The device involves separate measurements of CO_2 and soot mass concentrations and can report an emissions index stated in grams of soot per kilogram of fuel burned under the operating condition which applies at the time of the measurement. The instrument response to CO_2 was calibrated in an absorption cell; comparison with theory indicated a broadband leakage of 0.02% through the CO_2 bandpass filter. This leakage can be eliminated by adding a second bandpass filter to the CO_2 channel. This will increase the sensitivity to CO_2 relative to interferences from soot or other species. A new calibration will be required, and should cover a wider range of CO_2 absorber thicknesses to cover diluted plume cases and increased density cases which result from low temperature plumes such as occur on the roof.

The theoretical absorption model was used to analyze the response variations which would result if any of three different filters was added. The first case was a narrow bandpass filter centered over the current filter's measured (when cooled) center wavelength (CWL), with CWL / FWHM of 4.180 / 0.050 μm. The second case was a slightly wider bandpass at a higher CWL, near the ν_3 bandcenter of CO_2, or 4.225 / 0.190 μm. The third case was a slightly wider bandpass centered over the current filter's measured CWL, with 4.180 / 0.100 μm. Broadband transmission was assumed negligible with the second filter in place, since the combined minimum transmission should be around 10^{-7} to 10^{-8}. In each case, the sensitivity to CO_2 increased due to the removal of background transmission. The second case shows the greatest increase in sensitivity because it is centered near the center of the ν_3 band, away from the wings. However, it also results in a stronger attenuation of the signal than does case three, which still decreases the transmitted signal by 66%. Case three was also the least sensitive to a small changes in CWL, such as might occur with changes in filter temperature or slight

misalignments. For these reasons, an additional filter was purchased from Spectrogon, with a specified CWL and FWHM of 4.190 and 0.075 μm, respectively.

Initial tests performed on engine exhaust confirmed that absolute concentrations are difficult to determine using extinction in a remote sensing configuration. However, the relative extinction caused by soot and CO_2 did give a reliable indication of the specific soot emissions index for a wide range of operating conditions. This measurement is useful as a means to identify highly-polluting vehicles which are well outside the norm compared to other vehicles operated under the same conditions.

Measurement accuracies for the laboratory roof tests could be increased by isolating the lamp source from line voltage fluctuations. A 12 volt car battery coupled to a continuously charging low-ripple DC power supply should eliminate most of the source intensity fluctuations and at the same time maintain a constant battery charge. The additional space and power requirements would not be significant compared to the mounting stand required for remote measurements, and hence do not add any additional restrictions to device portability. A temperature measurement near the actual exhaust port exit would also be useful. It might also be interesting to take the Bosch smoke number measurements right near the exhaust pipe exit rather than just downstream of the exhaust manifold; one would expect the correlation to be somewhat different.

A final modification would be the addition of a corner cube or similar angularly invariant retro-reflector. Such a device is insensitive to minor misalignments or vibrations in its angular orientation. This would facilitate alignment and ensure that the reflected beam would be normal to the interference filters. Such retro-reflectors are commercially available at reasonable cost.

Further calibration of the soot extinction against dilution tunnel measurements of mass concentrations should also be performed to determine the soot response more accurately. Tests are currently being conducted with the cooperation of the Metropolitan Transit Commission and the University of West Virginia as part of their evaluation of alternative fuel buses. We also hope to obtain information of the increased emissions

during transient accelerations and decelerations. Complete results are expected by November.

Assuming the results of the MTC tests are satisfactory, the device can then be tested on moving vehicles, using a portable generator to provide power if necessary. Preliminary design considerations for mounting the sensors have already been performed, and a prototype is being built. A trigger circuit will have to be built to trigger acquisition of the background and plume extinctions. This circuit will produce a trigger pulse when a vehicle interrupts a beam, in much the same way that optical trigger beams are used to detect people entering doorways. The chopping frequency of the source will probably have to be increased to several kilohertz to provide adequate time resolution for measuring the plume extinctions of moving vehicles.

The Nicollet Mall in downtown Minneapolis provides an optimum test location, since vehicle traffic is restricted to transit vehicles (city buses) and emergency vehicles. Collaboration with the Metropolitan Transit Commission (MTC) can further provide for buses of the same configuration with exhaust pipes at similar heights. In this way, variations in the emissions index of the same or similar vehicles can be calculated over a range of operating conditions. Other tests could also be conducted at on-ramps to freeways to measure truck emissions, possibly at weigh station locations such that information on vehicle load can be obtained. The support stands have been designed with the flexibility to measure stack emissions at heights up to 14 feet, which should cover the necessary range for over-the-road trucks.

REFERENCES

Banwell, C. N., 1983. *Fundamentals of Molecular Spectroscopy,* McGraw-Hill, New York.

Beaton, S. P., G. A. Bishop and D. H. Stedman, 1992. "Emission Characteristics of Mexico City Vehicles," *J. Air Waste Manage. Assoc.*, **42**(11), 1424-1429.

Bishop, Gary A. and Donald H. Stedman, 1990. "On-Road Carbon Monoxide Emission Measurement Comparisons for the 1988-1989 Colorado Oxy-Fuels Program," *Environ. Sci. Technol.*, **24**(6), 843-847.

Burch, Darrel E., D. A. Gryvnak, R. R. Patty and C. E. Bartky, 1969. "Absorption of Infrared Radiant Energy by CO_2 and H_2O. IV. Shapes of Collision-Broadened CO_2 Lines," *J. Opt. Soc. Am.*, **59**, 267-280.

Cadle, Steven H., Mark Carlock, Richard E. Gibbs, Denneth T. Knapp, Alan C. Lloyd and William R. Pierson, 1991. "CRC-APRAC Vehicle Emissions Modeling Workshop," *J. Air Waste Manage. Assoc.*, **41**(6), 817-820.

Cousin, C., R. Le Doucen, J. P. Houdeau, C. Boulet and A. Henry, 1986. "Air Broadened Linewidths, Intensities, and Spectral Line Shapes for CO_2 at 4.3 μm in the Region of the AMTS Instrument," *Appl. Opt.*, **25**(14), 2434-2439.

Devi, V. Malathy, B. Fridovich, G. D. Jones and D. G. S. Snyder, 1984. "Diode Laser Measurements of Strengths, Half-Widths, and Temperature Dependence of Half-Widths for CO_2 Spectral Lines near 4.2 μm," *J. Mol. Spectrosc.*, **105**, 61-69.

Eskridge, Robert E., William B. Petersen and S. Trivikrama Rao, 1991. "Turbulent Diffusion Behind Vehicles: Effect of Traffic Speed on Pollutant Concentrations," *J. Air Waste Manage.*, **41**(3), 312-317.

Hänel, G., 1988. "Single Scattering Albedo, Asymetry Parameter, Apparent Refractive Index and Apparent Soot Content of Dry Atmospheric Particles," *Appl. Opt.*, **27**(11), 2287-2295.

Hansen, A. D. A. and H. Rosen, 1990. "Individual Measurements of the Emission Factor of Aerosol Black Carbon in Automobile Plumes," *J. Air Waste Manage. Assoc.*, **40**(12), 1654-1657.

Haskew, H. M., J. J. Gumbleton, and D. P. Garrett, 1987. "I/M Effectiveness with Today's Closed Loop Systems," *SAE Tech. Paper Ser.*, No. 871103.

Heywood, John B., 1988. *Internal Combustion Engine Fundamentals*, McGraw-Hill, New York.

Hofeldt, David L., 1993a. Private communication.

Hofeldt, David L., 1993b. "Real-Time Soot Concentration Technique for Engine Exhaust Streams," *SAE Tech. Paper Ser.*, No. 930079.

Ingalls, M. N., 1989. "On-Road Vehicle Emissions Factors form Measurements in a Los Angeles Area Tunnel," Paper No. 89-137.3, presented at the A&WMA 82nd Annual Meeting, Anaheim, CA.

Johns, J. W. C., 1987. "Absolute Intensity and Pressure Broadening Measurements of CO_2 in the 4.3-μm Region," *J. Mol. Spectrosc.*, **125**, 442-464.

Kittelson, David B., Paul A. Kadue, Huel C. Scherrer and Rex E. Lovrien, 1988. *Characterization of Diesel Particles in the Atmosphere,* Final Report submitted to Coordinating Research Council AP-2 Project Group.

Kittelson, D. B., I. S. Abdul-Khalek, Y. Chen, C.-J. Du, D. J. Haugen, and E. Stenersen, 1994. "Influence of a Fuel Additive on the Performance and Emissions of a Medium-Duty Diesel Engine," *SAE Tech. Paper Ser.*, No. 941015.

Knapp, Kenneth T., 1991. "Dynamometer Testing of On-Road Vehicles from the Los Angeles In-Use Emissions Study," U. S. Environmental Protection Agency, Atmospheric Research and Exposure Assessment Laboratory, Research Triangle Park, NC 27711.

Lawson, Douglas R., Peter J. Groblicki, Donald H. Stedman, Gary A. Bishop and Paul L. Guenther, 1990. "Emissions from In-Use Motor Vehicles in Los Angeles: A Pilot Study of Remote Sensing and the Inspection and Maintenance Program," *J. Air Waste Manage. Assoc.*, **40**(8), 1098-1105.

Liu, B. Y. H., 1976. Class notes for Particle Technology, University of Minnesota, Minneapolis.

Menoux, V., R. Le Doucen and C. Boulet, 1987. "Line Shape in the Low-Frequency Wing of N_2 and O_2 Broadened CO_2 Lines," *Appl. Opt.*, **26**(23), 5183-5189.

Novakov, T., 1982. "Soot in the Atmosphere." *Particulate Carbon: Atmospheric Life Cycle,* Ed. George T. Wolff and Richard L. Klimisch, Plenum Press, New York. 19-37.

Prochnau, T. J., 1994. "Development of a Remote Sensing System for Measuring Particulate Emissions from Heavy-Duty Vehicles," Master's Thesis, Dept. of Mechanical Engineering, University of Minnesota, April 1994.

Rueff, Roger M., 1992. "The Cost of Reducing Emissions from Late-Model High-Emitting Vehicles Detected Via Remote Sensing," *J. Air Waste Manage. Assoc.*, **42**(7), 921-925.

Scherrer, Huel C., David B. Kittelson and Daniel F. Dolan, 1981. "Light Absorption Measurements of Diesel Particulate Matter," *SAE Tech. Paper Ser.*, No. 810181.

Scherrer, Huel C. and David B. Kittelson, 1994. "I/M Effectiveness as Directly Measured by Ambient CO Data," *SAE Tech. Paper Ser.*, No. 940302.

Seinfeld, John H., 1986. *Atmospheric Chemistry and Physics of Air Pollution,* John Wiley & Sons, New York.

Society of Automotive Engineers, 1994. *1994 SAE Handbook*, Society of Automotive Engineers, Warrendale, PA, pp. XXX.

Stephens, Robert D. and Steven H. Cadle, 1990. "Remote Sensing Measurements of Carbon Monoxide Emissions from On-Road Vehicles," General Motors Research Laboratories, Publication GMR-7030.

Stephens, Robert D. and Steven H. Cadle, 1991. "Remote Sensing Measurements of Carbon Monoxide Emissions from On-Road Vehicles," *J. Air Waste Manage.*, **41**(1), 39-46.

U.S. Environmental Protection Agency, 1993. "User's Guide to MOBILE5a (Mobile Source Emission Factor Model)," U.S. EPA, National Vehicle and Fuel Emissions Laboratory, Emission Planning & Strategies Division, Air Quality Analysis Branch, Ann Arbor, MI 48105.

White, John U., 1942. "Long Optical Paths of Large Aperture," *J. Opt. Soc. Am.*, **32**, 285-288.

Young, Hugh D., 1962. *Statistical Treatment of Experimental Data*, McGraw-Hill, New York, p. 100.

APPENDIX A: NOTATION

SYMBOL	QUANTITY	UNITS
A_{abs}	mass-specific absorption cross section	m^2/g
A_{ext}	mass-specific extinction cross section	m^2/g
A_{sca}	mass-specific scattering cross section	m^2/g
A_{det}	detector area	m^2
A_s	source area	m^2
BSC	brake-specific particulate emission	g/bhph
BSFC	brake-specific fuel consumption	g/bhph
D_p	equivalent particle diameter	μm
$D^*(\lambda)$	detectivity	cm $Hz^{1/2}/W$
$e_\lambda(T)$	blackbody spectral emittance	W/m^2 μm
$e_\nu(T)$	blackbody spectral emittance	W/m^2 cm^{-1}
EI_{PM}	emissions index of particulate matter	g C/kg fuel
FC	fuel consumption	mi/gal
G_{amp}	transimpedance gain	V/A
I_ν	resultant spectral intensity	W/m^2 cm^{-1}
$I_{\nu o}$	incident spectral intensity	W/m^2 cm^{-1}
I_λ	resultant spectral intensity	W/m^2 μm
$I_{\lambda o}$	incident spectral intensity	W/m^2 μm
I_{sig}	total detector current output	A
$I_{sig,\lambda}$	detector current output per unit wavelength	A/μm
$k_i(\nu)$	absorption coefficient for individual line	cm^{-1}/atm
L	optical pathlength	cm, m
L_a	optical pathlength in ambient	m
L_p	optical pathlength through plume	m
L_{tot}	total optical pathlength	m
$\dot{m}_{co2}$	mass flow rate of CO_2 in exhaust	g/s
$\dot{m}_f$	mass flow rate of fuel	g/s
M	mass concentration of carbonaceous soot	g/m^3
M_a	ambient mass concentration of particles	g/m^3

SYMBOL	QUANTITY	UNITS
M_C	atomic mass of C	g/mol
M_{CO}	molecular mass of CO	g/mol
M_{CO2}	molecular mass of CO_2	g/mol
M_{ex}	molecular mass of exhaust gas	g/mol
M_f	molecular mass of fuel	g/mol
M_m	molecular mass of absorbing gas	g/mol
M_p	mass concentration of particles in plume	g/m^3
MMD	particle mass mean diameter	μm
p_a	partial pressure of absorbing gas	atm
Q_1	molar ratio of CO/CO_2	
Q_2	molar ratio of HC/CO	
Q_3	molar ratio of CO/C	
$R(\lambda)$, $R(\nu)$	spectral responsivity of detector	A/W
R_u	universal gas constant	82.04 atm cm^3/mol K
S_i	linestrength	cm^{-1}/atm
T	source temperature	K
T_o	reference temperature	K
V_{ref}	reference signal voltage	V
V_{sig}	signal voltage	V
VEI_{CO}	vehicle CO emissions index	g CO/mi
x_{co2}	volume fraction of CO_2 in exhaust	
y_{cf}	mass fraction of C in fuel	
$\alpha(\nu)$	absorption coefficient	cm^{-1}
$\beta(\nu)$	absorption coefficient	m^2/g
$\chi(\nu-\nu_{o,i})$	lineshape correction factor	
$\varepsilon_s(\lambda)$, $\varepsilon_s(\nu)$	source emissivity	
ϕ	equivalence ratio	
γ_i	line full-width half-maximum	cm^{-1}
γ^o_i	gas broadening coefficient	cm^{-1}/atm

SYMBOL	QUANTITY	UNITS
η_i	chemical equation coefficients	
$\eta(\lambda)$, $\eta(\nu)$	efficiency of transmissive and reflective optics	
$\eta_{bp}(\nu)$	efficiency of bandpass filter	
$\kappa(\nu)$	absorption coefficient	cm^{-1}/atm
λ	wavelength	μm
ν	wavenumber	cm^{-1}
ν_i	fundamental molecular vibration modes	cm^{-1}
$\nu_{o,i}$	line center	cm^{-1}
ρ	gas density	g/m^3 or kg/m^3
ρ	particle density	g/cm^3
ρ_{CO2}	mass density of CO_2 gas	g/m^3 or kg/m^3
ρ_f	fuel density	g/gal
σ_g	geometric width of log-normal distribution	
Ω	solid angle collected by detector	steradians

APPENDIX B: DETAILED EXTINCTION THEORY

B.1 EXTINCTION BY PARTICULATES

Optical extinction by particulates is comprised of both scattering and absorption components, and is a complicated function of the spectral region and the size of the particles. The scattering part is very size dependent; for example, the mass-specific absorption cross section varies with the first to third power of diameter, depending on the particle size and illumination wavelength. Hence, scattering does not make a very good soot diagnostic, since the exact size distribution is not known. Absorption is proportional to the particle volume, and hence mass, and is relatively insensitive to variations in the particle size distribution. At visible and near infrared wavelengths, absorption by soot is dominated by the amount of amorphous carbon, and volatiles play only a small role. Fortunately, extinction by soot at visible and near infrared wavelengths is dominated by absorption, which accounts for about 67% of the total extinction at $\lambda = 0.532$ μm and increases to more than 95% at $\lambda = 4.2$ μm. With a judicious choice of wavelength near 630 nm, the extinction is essentially independent of variations in size distributions typical of diesel engines. Hence, extinction near 630 nm makes a good diagnostic of the mass concentration of the carbonaceous portion of the diesel particulates.

Optical extinction follows the Beer-Lambert Law, which for particles of a given size can be written as

$$I_\lambda = I_{\lambda o}\, e^{-A_{ext}(\lambda, D_p)\, M\, L} \quad , \tag{B.1}$$

where λ is the wavelength (μm), D_p is the equivalent spherical particle diameter (μm), $I_{\lambda o}$ is the incident spectral intensity (W/m^2-μm), $A_{ext}(\lambda, D_p)$ is the mass-specific extinction cross section (m^2/g), M is the total mass concentration of carbonaceous soot (g/m^3), L is the pathlength (m), and I_λ is the transmitted spectral intensity (W/m^2-μm).

Equation (B.1) is really a summation of the energy loss due to scattering and aborption by many individual particles. Let us write the extinction of energy from a beam

in terms of the fraction of the beam area A "blocked" by a single particle whose extinction cross section is C_{ext}:

$$\frac{I}{I_0} = \exp\left[-\frac{C_{ext}}{A}\right] \tag{B.2}$$

As long as multiple scattering isn't important, the extinction from n such particles contained anywhere in the beam path can be written as

$$\ln\left(\frac{I}{I_0}\right) = -n\frac{C_{ext}}{A} \tag{B.3}$$

The numerator and denominator of the right hand side of (B.3) can then be multiplied by the path length, L, and then we can make a substitution to include the particle number density, $N = n/(AL)$:

$$\frac{I}{I_0} = \exp\left[-NC_{ext}L\right] \tag{B.4}$$

Multiplying N and dividing C_{ext} by the mass per particle gives the form shown in (B.1), which is more convenient when considering soot emissions which are regulated in terms of mass.

In general, a distribution of particles will be illuminated by the source, and since A_{ext} depends on both λ and D_p, we need to integrate over the source spectrum and the particle size distribution. Confining our attention for now to a single wavelength λ, we can extend the derivation given above for a distribution of particles; the result is

$$\frac{I_\lambda}{I_{\lambda o}} = \exp\left[-\int_{D_p} A_{ext}\, g(D_p)\, M\, L\, dD_p\right]$$

$$\frac{I_\lambda}{I_{\lambda 0}} = \exp\left[-M\, L \int_{D_p} g(D_p)\, A_{ext}\, dD_p\right], \tag{B.5}$$

where $I_{\lambda 0}$ and I_λ are the spectral intensities at wavelength λ [W/m^2] at the beginning and end of the path, respectively, and $g(D_p)$ is the normalized mass probability distribution function.

The quantity in the integral is just the average value of the exintction coefficient for the size distribution,

$$\bar{A}_{ext}(\lambda, g(D_p)) = \int_{D_p} g(D_p)\, A_{ext}(\lambda, D_p)\, dD_p \ , \tag{B.6}$$

so the extinction can be written as

$$\frac{I_\lambda}{I_{\lambda 0}} = \exp\left[-\bar{A}_{ext} M L\right] \ . \tag{B.7}$$

If the exponent argument (in [ ]) is small for all particle sizes, then it can be expanded as

$$\exp[-x] \approx 1 - x \ . \tag{B.8}$$

Eqn. B.6 then simplifies to

$$\frac{I_\lambda}{I_{\lambda o}} \approx 1 - \bar{A}_{ext} M L \ , \tag{B.9}$$

and the extinction is linear in ML. The expansion is termed the optically thin limit, and is accurate to better than 5.5% as long as the argument is less than 0.3.

Figures B.1(a) and B.1(b) show $\bar{A}_{ext}$ versus mass median particle diameter (MMD) for different wavelengths in the visible and mid-infrared regions, respectively. Two curves are shown for each wavelength: one for a relatively narrow size distribution with a geometric standard deviations of $\sigma_g = 1.75$ ($ln\ \sigma_g = 0.56$), and another for a wider distribution with $\sigma_g = 1.90$ ($ln\ \sigma_g = 0.64$). The values were calculated from Lorenz-Mie theory assuming the soot particles have an effective density $\rho = 1$ g/cm^3. For a fixed size distribution, $\bar{A}_{ext}$ is greater for lower λ; thus a lower λ allows greater sensitivity to the presence of soot. However, because scattering becomes more important at shorter wavelengths, the signal will be more sensitive to variations in the particle distribution.

In order to measure the mass concentration of soot particles emitted from diesel vehicles with a remote sensing system, we want the extinction to be essentially independent of size and composition variations typical of diesel engines. Particulate distributions are typically log-normal with mass median diameters (MMD) between about 0.2-0.3 μm and geometric standard deviations (σ_g) in the range of 1.7-2.0 [Kittelson et al. 1988]. For these size ranges, $\bar{A}_{ext}$ is nearly independent of particle size for wavelengths

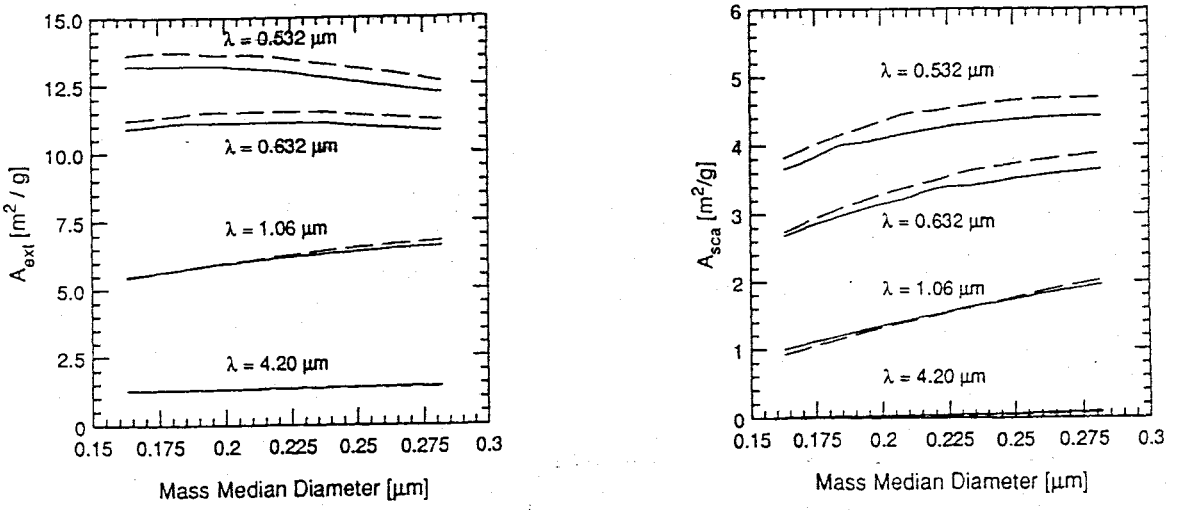

Fig. B.1: Average mass specific (a) extinction and (b) scattering cross sections for dry soot as a function of particle size and wavelength. The values are integrated over lognormal size distributions and plotted versus mass median diameter for several distribution widths typical of diesel engines at various operating conditions. The dashed lines are for σ_g=1.75 and the solid lines are for σ_g=1.90

near 0.63 μm, which is in the red region of the spectrum. At both shorter and longer wavelengths, $\overline{A}_{ext}$ can vary by about 10% over the range of size distributions typical of diesel engines. Alternatively, one could achieve size distribution independence by summing the extinction in two bandwidths, one in which A_{ext} increased with increasing particle size and the other where A_{ext} decreased with increasing particle size. The total extinction would then be independent of particle size distribution. Ratioing the extinction or scattering in the two detection bandwidths could then also be used to obtain information on the particle size distribution [Hofeldt, 1993a and 1993b].

Figure B.1 also shows the effective mass-specific single scattering cross section for dry soot versus mass median diameter, $\overline{A}_{sca}$. We caution that this curve is not valid if

volatiles are condensed on the soot. The single scattering assumption is valid if the aerosol is optically thin with respect to scattering such that the probability of light rays being scattered off more than one particle is small. This is assured if $\overline{A}_{sca}ML < 0.1$ for all particle sizes. However, if $\overline{A}_{sca}ML > 0.3$, scattering is significant, and multiple scattering may cause some of the light initially scattered out of the beam to be scattered back toward the detector in subsequent scattering events, thereby increasing signal levels. An extinction measurement in such cases would underpredict the particle mass concentration. In the red part of the visible spectrum, scattering in all directions accounts for about 30% of the total extinction; of this 30%, a subsequent scattering event would scatter some light back toward the detector. However, the theory assumes there is no contribution due to multiple scattering. Hence, multiple scattering increases the observed signal, and an extinction measurement would underpredict the mass concentration. The increase in signal can be significant, especially when spatial variations in M exist along the path. However, the effect is largely damped in strongly absorbing particle fields since the scattered light is subject to absorption between the first and second scattering events as well as on its way to the detector, such that much of the multiply scattered energy would be lost. Still, since the effects of multiple scattering are difficult to know in advance, it is best to avoid the multiple scattering regime and operate with $\overline{A}_{sca}ML < 0.3$.

If the light is polychromatic (literally, it consists of more than one color, i.e. wavelength), then the light reaching the detector must be summed over each wavelength element. Since the extinction coefficient varies with lambda, the resultant differential intensity dI [W/m^2] within a wavelength interval dλ about λ which reaches the detector after passage through the particle field is

$$dI(\lambda) = I_\lambda \, d\lambda = I_{\lambda o} \, \exp\left[-\overline{A}_{ext}(\lambda, g(D_p)) \, M \, L\right] d\lambda \quad . \tag{B.10}$$

To integrate the detector response, we must also account for variances in the spectral profiles of all the other optical components in the system, including the source or sources, reflective optics, transmitting optics, and detector. If an incandescent source characterized by an emissivity $\varepsilon(\lambda)$ and a spectral emittance $e_\lambda(T)$ [W/m^2/μm] provides the illumination, the optics are characterized by a net transmission efficiency of $\eta_1(\lambda)$, and the

detector has an area A_{det} [m^2] and responsivity $R_1(\lambda)$ [A/W], then the differnetial current output for a differential wavelength range centered at λ is

$$I_{sig,\lambda}\, d\lambda = R_1(\lambda)\, \eta_1(\lambda)\, [\frac{\Omega}{4\pi} A_s\, \varepsilon_s(\lambda)\, e_\lambda(T)] \exp[-\bar{A}_{ext} ML]\; d\lambda \quad . \tag{B.11}$$

Here, T is the source temperature [K], and the source area, A_s [m^2], and solid angle, Ω [steradians], define the light which is recieved at the detector. The total current produced by the detector is the integral of (B.11) over all λ:

$$I_{sig} = \int_\lambda R_1(\lambda)\, \eta_1(\lambda)\, [\frac{\Omega}{4\pi} A_s\, \varepsilon(\lambda)\, e_\lambda(T)]\; \exp[-\bar{A}_{ext} ML]\; d\lambda \quad . \tag{B.12}$$

Usually the detector signal is passed through a preamplifier with a transimpedance gain G_{amp} (V/A); the signal voltage dependence is then

$$V_{sig} = G_{amp} \frac{\Omega}{4\pi} A_s \int_\lambda R_1(\lambda)\eta_1(\lambda)\varepsilon(\lambda) e_\lambda(T)\; \exp\left[-ML \int_{D_p} g(D_p) A_{ext}(\lambda, D_p)\, dD_p \right] d\lambda \tag{B.13}$$

To simplify the notation, we define a normalized spectral illumination and response function $f(\lambda)$ as

$$f(\lambda) = \frac{R_1(\lambda)\, \eta_1(\lambda)\, \varepsilon(\lambda)\, e_\lambda(T)}{\int_\lambda R_1(\lambda)\, \eta_1(\lambda)\, \varepsilon(\lambda)\, e_\lambda(T)\, d\lambda} \tag{B.14}$$

Then, (B.13) can be written as

$$V_{sig} = C \int_\lambda f(\lambda)\; \exp\left[-ML \int_{D_p} g(D_p) A_{ext}(\lambda, D_p)\, dD_p \right] d\lambda \;, \tag{B.15}$$

where C is a proportionality constant. The ratio of this signal to one obtained at a different time with M=0 or L=0 is given by

$$\frac{V_{sig}}{V_0} = \int_\lambda f(\lambda)\; \exp\left[-ML \int_{D_p} g(D_p) A_{ext}(\lambda, D_p)\, dD_p \right] d\lambda \tag{B.16}$$

as long as all of the other factors affecting C remain constant in the interval between measurements.

As before, ML can only be taken outside the exponent in the limit that the extinction at all wavelengths is optically thin. In this limit, we can show that

$$\frac{V_{sig}}{V_0} \approx 1 - A_{e,eff}(f(\lambda), g(D_p))ML \tag{B.17}$$

where

$$A_{e,eff}(f(\lambda), g(D_p)) = \int_{\lambda} f(\lambda)\bar{A}_{ext}(\lambda, g(D_p))\, d\lambda \quad . \tag{B.18}$$

Again, we emphasize that (B.17) only holds in the optically thin limit; if at some wavelength the extinction is optically thick, then other wavelengths which are optically thin will preferentially weight the detected signal.

For a given optical configuration, all of the parameters in equation (B.13) except those in the exponent are assumed to remain constant in the short time before and after an exhaust plume interrupts the beam. A_{ext} is fixed by the properties and size distribution of the aerosol; we have already discussed how to choose the wavelength such that the size-averaged extinction is nearly constant for typical soot distributions. Thus, ML, the mass concentration-pathlength product (also called the absorber thickness), determines how the signal responds to a passing plume. High values of A_{ext} make it easier to detect the signal change at low concentrations (low M), but they also reduce the sensitivity to variations in M at high concentrations (progressively larger changes in M are required to produce the same change in signal).

In both cases, the change in signal compared to the inherent system noise determines the accuracy of the measurement, so the wavelength region employed must be a compromise to achieve good detectability and adequate dynamic range. Furthermore, we need to avoid the multiple scattering regime, *i.e.* $A_{sca}M_{max}L < 0.3$, which for red wavelengths would imply $A_{ext}M_{max}L < 1$. One can always wait for a short time for the plume to disperse enough that this limit can be avoided. However, since the plume from a passing vehicle presents a signal which varies fairly rapidly with time, we can't employ lock-in amplification or signal averaging techniques with long time constants to pick out very weak absorptions. Hence, detecting a 1% absorption might be about the best one could expect to do in a field measurement. Thus, the dynamic range of accurate measurements of M might be about two orders of magnitude, but because we can wait for

dispersion to dilute higher concentrations, it is more important to ensure adequate sensitivity for accurate measurements of low concentrations.

Recall that we also wish to choose the wavelength such that the extinction is independent of size variations, and that 630 nm was a good choice. Hence, we need to determine what path length would be needed to detect extinction at 630 nm for the smallest desired value of M. From Fig. B.1, we see that a typical diesel plume would have $A_{ext} = 11$ m^2/g at 630 nm. State-of-the-art engines running under light load conditions could yield concentrations as low as 3 mg/m^3, while full load conditions would produce closer to 30 mg/m^3. Older engines may be 3-5 times dirtier, and fuel rich acceleration transients can easily produce concentrations in excess of 500 mg/m^3.

A double pass across an undiluted 5 mg/m^3 exhaust plume from a 4" diameter exhaust pipe gives $L = 0.2$ m and would result in 1.1% extinction, while four passes ($L =$ 0.4 m) would produce 2.2% extinction. In the double pass configuration, a plume particle concentration of $M_p < 136$ mg/m^3 would still be optically thin, whereas four passes through a similar plume with $M_p = 68$ mg/m^3 would yield $\bar{A}_{ext}ML = 0.3$. With $M_p = 500$ mg/m^3, only 33% of the light would be transmitted (67% extinction) through the plume in two passes, which should also be at the threshold of multiple scattering. For the four pass configurations, we would have to wait for some dilution of the plume to avoid multiple scattering for concentrations exceeding 227 mg/m^3. The difference between the absolute and relative accuracies at these extreme values of M can be illustrated by noting that a mass concentration of 10 mg/m^3 results in 2% extinction, whereas a mass concentration of 518 mg/m^3 results in a 68% extinction.

Finally, (B.17) indicates that a ratio needs to be taken to cancel out all factors except the soot mass concentration. Because a ratio is taken, the change in signal caused by the plume mass concentration must be significant compared to noise on the signal with or without the plume. This can be seen if we assume V_1 and V_2 represent the signals before and within the plume, with rms noise levels of σ_1 and σ_2. Analysis of the propagation of the errors [Young, 1962] then leads to

$$\left(\frac{\sigma_Q}{Q}\right)^2 = \left(\frac{\sigma_1}{V_1}\right)^2 + \left(\frac{\sigma_2}{V_2}\right)^2 \qquad \text{(B.19)}$$

where σ_Q represents the standard deviation of the quotient $Q=V_2 / V_1$. Equation (B.4) can be simplified for the case of $\sigma_1 = \sigma_2 = \sigma_{ms}$ to $(\sigma_Q / Q)^2 = (1 + Q^2)\ (\sigma_{ms} / V_2)^2$. Note that the fractional standard deviation of the quotient has increased by the factor $(1 + Q^2)^{1/2}$ over the fractional standard deviation of the V_2 signal. Since both the soot and CO_2 concentrations are calculated from ratios in this manner, the noise on both signals determine the accuracy of the computed emissions index.

B.2 ABSORPTION BY CO_2

CO_2 is a linear triatomic molecule which has infrared emission and absorption bands. Infrared emission or absorption occurs when there is periodic fluctuation in the molecular dipole moment, as a result of vibrations of the individual atoms which comprise the molecule. A linear triatomic configuration allows three fundamental modes of vibration: symmetric stretching, bending, and antisymmetric stretching, occurring at wavenumbers ν_1, ν_2, and ν_3, respectively. (Note: infrared spectroscopy generally uses wavenumber notation, denoted by the symbol ν (cm^{-1}) in this work). In addition to the fundamental modes are combination and difference bands, eg. $\nu_1 - \nu_2$, which in general exhibit much less emission and absorption and are not considered here. For the symmetric stretch mode, there is no change in the dipole moment during the vibration; therefore, this mode is not "infrared active" [Banwell 1983]. For CO_2, modes ν_2 and ν_3 occur at 667 cm^{-1} and 2349 cm^{-1} (15.0 μm and 4.26 μm), respectively. More sources and detectors are available for 2349 cm^{-1}, and thus the ν_3 vibration is better suited for remote sensing purposes.

Absorption and emission associated with the fundamental vibration modes ν_i are not single frequencies but rather the centers of bands of individual lines. These individual lines result when the molecule makes a transition from one rotational energy level to another. Each line has an associated profile or lineshape in frequency space. Three broadening mechanisms of interest contribute to the lineshapes: natural broadening,

Doppler broadening, and collision broadening. Natural broadening occurs as a result of the Heisenberg uncertainty principle; the uncertainty in the energy difference between two energy levels or states leads to a corresponding uncertainty in the line frequency, resulting in line broadening, and a line profile which is described by a Lorentzian function. The natural-broadening of infrared transitions is generally negligible compared to other broadening mechanisms.

Doppler line broadening occurs because the molecules are in motion and emitted or absorbed radiation exibits Doppler shifts in frequency; shifts occur to both higher and lower frequencies, broadening the line. The result of Doppler broadening is a Gaussian lineshape profile. For typical ambient temperatures, a Doppler-broadened line in the ν_3 band of CO_2 will also have a FWHM around 10^{-3} cm^{-1}.

Collisional broadening results from the collisions between molecules, which perturb the molecular energy levels. The shape of a collision-broadened line is also Lorentzian. For typical ambient temperatures and pressures, a collision-broadened line within ν_3 of CO_2 will be around 0.1 cm^{-1}. In general, the lineshape of a molecular transition will be a convolution of the Lorentzian and Gaussian lineshapes; in our case, collision broadening dominates, and the effects of natural and Doppler broadening can be neglected.

Each line also has a line intensity, or linestrength, which will be defined shortly. The linestrength depends on the transition probability between states and the relative populations of states involved in the transition, but not the overall concentration of the sample. In effect, it is analogous to the amplitude of a wave.

Our goal is to relate the absorption in a particular wavelength band to the concentration of the molecules present which absorb in that region of the spectrum. To do this, we must take linewidths and linestrengths into account. It is convenient at this time to restate the Beer-Lambert Law for an absorbing gas at a particular frequency ν:

$$I_\nu = I_{\nu o}\, e^{-\alpha(\nu) L} = I_{\nu o}\, e^{-\kappa(\nu) p_a L \frac{T_o}{T}} \quad , \tag{B.20}$$

where $\alpha(\nu)$ (cm^{-1}) and $\kappa(\nu)$ (cm^{-1}/atm) are two ways of defining the absorption coefficient, p_a is the partial pressure (atm) of the absorbing gas, L is the pathlength (cm), T is the temperature (K) and T_o the reference temperature for $\kappa(\nu)$ [Burch et al. 1969]. Note: molecules do scatter radiation just like particles do, but the extinction within an absorption band will be dominated by the absorption, so we have simply adopted the standard notation and dropped the scattering altogether. The rightmost portion of (a.20) assumes that the gas is ideal.

The total absorption coefficient, $\kappa(\nu)$, represents the sum over the individual line absorption coefficients $k_i(\nu)$ (cm^{-1}/atm):

$$\kappa(\nu) = \sum_i k_i(\nu) \, . \tag{B.21}$$

The absorption coefficient of one line of a pure gas is given by

$$k_i(\nu) = \frac{\nu}{\nu_{o,i}} \frac{S_i}{\pi} \frac{\gamma_i \, \chi(\nu - \nu_{o,i})}{\gamma_i^2 + (\nu - \nu_{o,i})^2} \quad , \tag{B.22}$$

where

$$S_i = \int_\nu k_i(\nu) \, d\nu \, , \tag{B.23}$$

is the linestrength (cm^{-2}/atm), $\nu_{o,i}$ is the line center, γ_i is the collision-broadened FWHM of the line (cm^{-1}), and $\chi(\nu-\nu_{o,i})$ is an empirically-determined shape correction factor to the Lorentzian lineshape [Menoux et al. 1987]. Collision broadening within a pure gas is called self-broadening. For a gas mixture, (B.22) is replaced by

$$k_i(\nu) = \frac{\nu}{\nu_{o,i}} \frac{S_i}{\pi} \frac{\gamma_i^0 \, p_a \, \chi(\nu - \nu_{o,i}) + \Sigma_b \, \gamma_{b,i}^0 \, p_b \, \chi_b(\nu - \nu_{o,i})}{\gamma_i^2 + (\nu - \nu_{o,i})^2} \quad , \tag{B.24}$$

$$\gamma_i = \gamma_i^0 \, p_a + \sum_b \gamma_{b,i}^0 \, p_b \, ,$$

where γ^0_i is the self broadening coefficient (cm^{-1}/atm) and the subscript b refers to the broadening gases. The temperature dependence of γ^0_i is given by

$$\gamma_i^0(T) = \gamma_i^0(T_o) \, [\frac{T_o}{T}]^n \, , \tag{B.25}$$

where n is generally 0.75 [Cousin et al. 1986].

For CO_2 in air or exhaust gas, the broadening gases are essentially just N_2, O_2, H_2O, and CO_2. However, the broadening coefficients for O_2 are nearly the same as for N_2, and H_2O and CO_2 are at relatively low concentrations in diesel exhaust, so the broadening coefficients are usually approximated with those of N_2. Line centers, linewidths, and linestrengths have been tabulated from various measurements found in spectroscopic literature, making it possible to calculate the total absorption coefficient $\kappa(\nu)$. (In addition to references already cited, see also Devi, *et al.* 1984; Johns, 1987; and Menoux, *et al.*, 1987.)

The factor p_a/T in (B.20) can be replaced by the absorbing gas density, ρ_a, via the ideal gas law:

$$I_\nu = I_{\nu o}\, e^{-\kappa(\nu)\, p_a\, L\, \frac{T_o}{T}} = I_{\nu o}\, e^{-\beta(\nu)\, \rho_a\, L}, \tag{B.26}$$

$$\beta(\nu) = C\, \frac{R_u T_o}{M_a}\, \kappa(\nu), \tag{B.27}$$

where $\beta(\nu)$ is the absorption coefficient (m^2/g), $C = 10^{-4}$ (m^2/cm^2), ρ_a is the mass density of the absorbing gas (species *a*) (g/m^3), R_u is the universal gas constant (82.04 atm cm^3/mol K), M_a is the molecular weight of gas *a* (g/mol), and L is the pathlength (m). Thus, a detector sensitive to ν_3 of CO_2 and subject to the same optical setup as described for (B.13) will produce an amplified voltage signal

$$V_{sig} = G_{amp}\, \frac{\Omega}{4\pi}\, A_s \int_\nu R_2(\nu)\, \eta_2(\nu)\, \varepsilon(\nu)\, e_\nu(T)\, e^{-\beta(\nu)\, \rho_{CO2}\, L}\, d\nu, \tag{B.28}$$

where the wavelength integration has been replaced by the corresponding wavenumber integral. In writing (B.28), we have explicitly allowed for different detector response and optics transmission functions than those employed in the particulate detection, but have indicated the use of the same source.

Equation (B.28) is for absorption by CO_2 in air and does not account for the presence of particulates. Since soot particles absorb and scatter energy over a broad spectral region, they will also contribute to the loss of light within the CO_2 band. The total

extinction is then the sum of contributions from the CO_2 absorption and the particulate extinction integrated over the detection band:

$$V_{sig} = G_{amp} \frac{\Omega}{4\pi} A_s \int_\nu R_2(\nu)\, \eta_2(\nu)\, \varepsilon(\nu)\, e_\nu(T)\, e^{-[\beta(\nu)\, \rho_{CO2}\, L + A_{ext}(\nu)\, M\, L]}\, d\nu \qquad \text{(B.29)}$$

The bandwidth of the CO_2 measurement must be kept small in order to avoid absorption by other gas species and to increase the sensitivity to CO_2 (wavelengths which are not absorbed by CO_2 only lead to a large background signal at the detector). This is accomplished by means of one or more interference filters which give rise to a transmission function $\eta_2(\nu)$. The gas absorption coefficient $\beta(\nu)$ still varies in a complicated fashion within the band transmitted by the interference filter, but the responsivity, source emissivity and intensity, and the particulate absorption factors remain essentially constant and their values at band center ν_3 can be pulled outside the integral:

$$V_{sig} = G_{amp} \frac{\Omega}{4\pi} A_s\, R_2(\nu_3)\, \varepsilon(\nu_3)\, e_\nu(T, \nu_3)\, e^{-[\bar{A}_{ext}(\nu_3)\, M\, L]} \int_\nu \eta_2(\nu)\, e^{-[\beta(\nu)\, \rho_{CO2}\, L]}\, d\nu \quad . \qquad \text{(B.30)}$$

The exponent within the bandpass integral cannot be expanded since many of the individual lines are not optically thin. Therefore, a calibration is necessary. This can be done in the laboratory with an absorption cell which allows variation of $\rho_{CO2}L$. It is important to ensure that the bandpass filter is oriented in the same manner in both the laboratory and on-road measurements or else the instrument response will change. The factors outside the integral can vary since they will cancel in the ratio below.

Following the aguments made in the particulate measurement section, a ratio between signals obtained with and without the plume will be required to remove drifts which may occur over time periods between vehicle measurements. Assuming $L_a = L_{tot}$, the ratio can be written as:

$$\frac{V_4}{V_3} = e^{-(\bar{A}_{ext}(\nu_3)\, M_p\, L_p)} \frac{\int_\nu \eta_2(\nu)\; e^{-\beta(\nu)\, [\rho_{CO2,a}\, L + \rho_{CO2,p}\, L_p]}\, d\nu}{\int_\nu \eta_2(\nu)\, e^{-\beta(\nu)\, \rho_{CO2,a}\, L}\, d\nu} \quad . \qquad \text{(B.31)}$$

Note that both the particulate and CO_2 concentrations in the plume affect the ratio (the ambient particulate extinction drops out to the limit that the plume does not change the

ambient path length). The previous section described how M_pL_p was to be determined; thus we will assume it is known. However, since the response curve is not purely exponential, the ratio may be different even though $\rho_{CO2,p}L_p$ remains the same if $\rho_{CO2,a}L_a$ changes. Since all we really want to know is $\rho_{CO2,p}L_p$, there are two ways to proceed: 1) monitor the ambient CO_2 concentration with a separate instrument, such that the plume concentration can be calculated from the signal ratio; or 2) periodically check the instrument calibration by inserting sample cells whose CO_2 concentration-pathlength products are known and which bracket the expected values of $\rho_{CO2,p}L_p$. The latter is effectively a field calibration of the instrument, which although more complicated, should be more accurate, since the former requires the assumption that the ambient CO_2 concentration is constant across the roadway.

Besides the interference from the particulate extinction, there are two additional subtle points to note about the CO_2 extinction measurements: 1) the absorption coeffiecient for the ambient CO_2 is essentially the same as that for the CO_2 in the plume, except for a small temperature effect, not significantly smaller as was the case for ambient particles; and 2) the absorption at some wavelengths within the detected band will be optically thick. The former is offset becase the ambient concentration of CO_2 is also relatively less, typically being on the order of 350 ppm. With regard to the second point, since the absorption at the centers of individual lines will be optically thick, most of the additional extinction due to CO_2 in the plume will come from the wings of the lines which are less optically thick; hence, factors which can affect the lineshape will be important.

The particulate and CO_2 measurements must be taken simultaneously such that both species have experienced the same dilution; we have implicitly assumed this by saying that M_pL_p was known above. The values for A_{ext} at the two different wavelength regions must also be known in order compute the appropriate value for M_pL_p from the soot measurement, and then to account for its extinction in the CO_2 measurement. This is an important limitation, since the variation in A_{ext} from visible to mid-infrared wavelengths has not been confirmed experimentally for a large number of engines or operating

conditions. Measuring the particulate concentration in a band nearer to the CO_2 band would reduce the uncertainty in A_{ext}, but the number of passes for the soot band might need to be incresed to achieve adequate sensitivity.

As with the soot measurement, it is important to ensure that the extinction produced by CO_2 in the plume lies within a reasonable range. CO_2 comprises roughly 10% by volume of the exhaust gas at full load, which corresponds to about 14% by mass. (For details of how to calculate these numbers, see section B.4; a typical full load equivalence ratio is ϕ=0.7.) If we assume the exhaust gas exits the stack at 500 °F (533 K), then the mass concentration (*i.e.* density) of CO_2 at the exhaust exit is about 100 g/m^3. The mass specific absorption coefficient of CO_2 over a relatively small spectral region surrounding 4.2 μm is about 9.6x10^{-3} m^2/g. (The spectral region is selected by a bandpass filter with a full-width at half-maximum (FWHM) passband of about 50 nm.) Thus, at full load with a double pass across a 4 inch exhaust pipe, we would measure about a 20% drop in signal.

Based on the discussion in the previous section, one might at first think this is too small for the full load case; however, one must recall that the CO_2 concentration is linear with fuel consumption, whereas soot concentration is not. Moreover, the range of CO_2 exhaust mass concentrations does not vary much from engine to engine. Hence, we only need to be able to measure CO_2 mass concentrations over a range of mass fractions of about 2 - 14% to be able to cover all operating conditions. Since the exhaust temperatures are cooler at light loads (approximately 400 °F = 478 K), the actual range of CO_2 mass concentrations in undiluted exhaust plumes is about 10 g/m^3 - 100 g/m^3. Hence, the extinction caused by the lowest CO_2 concentrations still lies above the 1% level used above.

B.3 EFFECT OF AMBIENT CONCENTRATIONS

The effect of background concentrations of particulates and CO_2 were discussed in detail in section 2.4 and do not need further elaboration here.

B.4 EMISSIONS INDICES

Thus far, we have only discussed ways to measure local soot and CO_2 absorber thicknesses, *i.e.* the product of local mass concentrations and path lengths. Assuming the two beam paths overlap and pass through the plume in the same number of passes, taking the ratio between the soot and CO_2 measurements would enable us to eliminate the unknown path length, leaving only the ratio of soot to CO_2. This section will show how such a ratio is a useful indicator of the soot output from a particular vehicle.

Vehicle emissions standards are indexed so that measurements from vehicles of different age, power, and weight operating under different loads will be comparable. However, the means by which regulated emissions are computed differ between light-duty and heavy-duty vehicles. Regulated light-duty vehicle emissions will be described first with an example before turning to heavy-duty vehicle emissions.

Consider regulations for light-duty CO emissions, which are specified in g/mile for a specific operating cycle. To measure this number, one needs to know the average mass of CO emitted per mile traveled during the cycle. This is readily done if the vehicle is on a chassis dynamometer or if it is instrumented to measure the CO mass output, but the measurement is not so simple for a random vehicle passing by a roadside checkpoint.

Current remote sensing devices calculate the regulated CO emissions index in the following manner. The sensor measures the molar ratio CO/CO_2 of a light-duty vehicle. Fuel economy is estimated by photographing the vehicle license plate, identifying the model from vehicle registration, and locating the fleet-average fuel economy rating for that model. The molar CO/HC ratio in the exhaust is sometimes also estimated from previously-measured averages. Finally, the fuel density is estimated by calculating the average local fuel density sold at the pumps. A carbon balance can then be performed for the fuel combustion process, where each carbon atom in the fuel is emitted in the exhaust as CO_2, HC, or CO (carbonaceous particulates are assumed negligible). The CO emissions in g/mi can only then be calculated from the measured CO/CO_2 ratio:

$$VEI_{CO} = \rho_f y_{cf} \frac{Q_1}{1+(1+Q_2)Q_1} \frac{M_{CO}}{M_C} \frac{1}{FC} = \rho_f y_{cf} Q_3 \frac{M_{CO}}{M_C} \frac{1}{FC}, \qquad \text{(B.32)}$$

Here VEI_{CO} is the regulated vehicle emissions index (g/mi), ρ_f is the fuel density (g/gal), y_{cf} is the mass concentration ratio of carbon to fuel, Q_1 is the molar ratio CO/CO_2, Q_2 is the molar ratio HC/CO, M_{CO} and M_C are the molecular and atomic masses of CO and C (carbon), respectively, FC is the fuel consumption (mi/gal), and Q_3 is the molar ratio CO/C [Stephens et al. 1990, 1991].

Note that a number of assumptions are required in order to obtain the value in terms of grams CO emitted per mile, of which the most important one is probably fuel economy. This assumption can be avoided if all we wish to measure is the amount of CO emitted per unit of fuel burned. This measure gives a direct indication of the efficiency of the engine and pollution control equipment on the vehicle, but doesn't penalize more powerful cars which tend to get poorer gas ~~mi~~leage. It is a valid emissions index, and in fact can always be used in conjunction with fleet fuel economy averages to obtain overall estimates for total mass emissions.

By contrast, heavy-duty vehicle emissions are regulated in g/bhp-hr, in order to allow for the broad range of power outputs from vehicles in this category. One would not expect an engine which produces 4 times the power output to produce the same total mass of emissions per unit distance traveled. Again, it is not easy to measure power output remotely; so we will define an emissions index instead. The mass concentration ratio of carbonaceous soot to CO_2 is readily calculated from the results of (B.13) and (B.31):

$$\frac{M_p}{\rho_{CO_2 p}} = \frac{M_p L_p}{\rho_{CO_2 p} L_p} \quad . \tag{B.33}$$

To calculate an emissions index one needs to know the ratio of the mass flow rate of CO_2 to the mass flow rate of fuel. This is given by

$$\frac{\dot{m}_{CO_2}}{\dot{m}_f} = \frac{\eta_{CO_2} M_{CO_2}}{\eta_f M_f} \quad , \tag{B.34}$$

where the η_i stand for the coefficients in the chemical equation relating products and reactants. Since diesel-fueled engines run lean, there will be very little CO, and one can assume that all C atoms in the fuel will be emitted in the exhaust as CO_2. This assumes, to

a first approximation, that the carbon content in carbonaceous soot and HC is also small compared to that in CO_2. This assumption can be checked by considering a vehicle which emits 10 times the allowed 1994 particulate matter standard of 0.1 g/bhp-hr; if its brake-specific fuel consumption (BSFC) is 0.25 kg/bhp-hr, and all the particulate matter is carbon, then for #2 (or light) diesel fuel only one out of every 217 carbon atoms ends up as particulate matter.

Thus #2 diesel fuel, given by $C_nH_{1.8n}$ ($n \cong 12$) [Heywood 1988], when burned completely undergoes the chemical reaction

$$\phi\, C_nH_{1.8n} + 6.921n(0.2095\, O_2 + 0.7808\, N_2 + 0.00935\, Ar + 0.00035\, CO_2) \quad \text{(B.35)}$$
$$\rightarrow\ n(\phi + 0.00242)\, CO_2 + 0.9\phi n\, H_2O + 1.45n(1-\phi)\, O_2 + 5.404n\, N_2 + 0.0647n\, Ar$$

where the equivalence ratio ϕ is defined as the ratio of actual to stoichiometric fuel-air mass ~~ratios~~:

$$\phi = \frac{(F/A)_a}{(F/A)_s}. \quad \text{(B.36)}$$

$\phi<1$ for diesel-fueled engines and varies with fuel flow rate, and hence engine load. We have included species with concentrations higher than 100 ppm for the composition of air. From (B.35), the volume fraction, x_{co2}, and mass fraction, y_{co2}, of CO_2 in the exhaust are

$$x_{co_2} = \frac{\phi + 0.00242}{6.921 + 0.45\phi} \quad \text{(B.37)}$$

and

$$y_{co_2} = x_{co_2}\frac{M_{co_2}}{M_{ex}}, \quad \text{(B.38)}$$

respectively, and the molecular weight of the exhaust gas, M_{ex} is

$$M_{ex} = \frac{200.5 + 13.83\phi}{6.921 + 0.45\phi}. \quad \text{(B.39)}$$

These quantities are useful for obtaining ρ_{co2}, the density of CO_2 in the exhaust.

From equation (B.34), we can find the mass ratio of CO_2 to fuel:

$$\frac{\dot{m}_{CO_2}}{\dot{m}_f} = \frac{(\phi n + 0.00242)\cdot 44.01}{\phi\,(12.01n + 1.811n)} \approx 3.19, \quad \text{(B.40)}$$

which depends on fuel type, but the difference between selecting #2 or #6 diesel (or heavy diesel, given by $C_nH_{1.7n}$ with n=14.6) is less than one percent. The emissions index for particulate matter follows from (B.40):

$$EI_{PM} = \frac{\dot{m}_{CO_2}}{\dot{m}_f} \frac{M_p}{\rho_{CO_2,p}} = 3.19 \frac{M_p L_p}{\rho_{CO_2,p} L_p} , \qquad \text{(B.41)}$$

The value is generally expressed in units of grams of particulate per kilogram of fuel burned. The emissions index allows comparison of particulate emissions from different vehicles with no additional assumptions other than fuel type. When combined with the mass of fuel burned in a region, it can also be used in computer models to estimate local pollution levels.

Equations (B.38) and (B.39) could be used together with the ideal gas law to substitute for ρ_{CO2} in (B.41) to obtain the emissions index as a function of equivalence ratio assuming the exhaust plume temperature at the location of the measurement was known. The measured emission indices could then be converted to brake-specific particulate carbon emissions (g/bhp-hr) by multiplying by the BSFC (g/bhp-hr), which is a fairly well known function of ϕ for different engines and operating conditions. This is similar to the need to assume a value for the fuel economy to obtain light-duty vehicle emissions in g/mile. We prefer to leave the result in terms of the measured particulate to CO_2 ratio,

$$BSC = 3.19\, BSFC \frac{M_p L_p}{\rho_{CO_2,p} L_p} . \qquad \text{(B.42)}$$

where we have been careful to use notation referring to carbon to distinguish it from the more standard notation of BSPM, which generally includes condensed volatiles.